Published in final edited form as:

Cancer Discov. 2016 June ; 6(6): 612–629. doi:10.1158/2159-8290.CD-16-0217.

BRD4 connects enhancer remodeling to senescence immune surveillance

Nilgun Tasdemir[1,2,3,7], **Ana Banito**[1,7], **Jae-Seok Roe**[3,7], **Direna Alonso-Curbelo**[1,7], **Matthew Camiolo**[4], **Darjus F. Tschaharganeh**[1], **Chun-Hao Huang**[1,5], **Ozlem Aksoy**[1,2,3], **Jessica E. Bolden**[1], **Chi-Chao Chen**[1,5], **Myles Fennell**[1], **Vishal Thapar**[1], **Agustin Chicas**[1], **Christopher R. Vakoc**[3,*], and **Scott W. Lowe**[1,6,*]

[1]Memorial Sloan-Kettering Cancer Center, New York, NY 10065, USA

[2]Watson School of Biological Sciences, Cold Spring Harbor, NY 11724, USA

[3]Cold Spring Harbor Laboratory, Cold Spring Harbor, NY 11724, USA

[4]Medical Scientist Training Program, Stony Brook University, NY 11794, USA

[5]Weill Graduate School of Medical Sciences, Cornell University, New York, NY10065, USA

[6]Howard Hughes Medical Institute, New York, NY 10065, USA

Abstract

Oncogene-induced senescence is a potent barrier to tumorigenesis that limits cellular expansion following certain oncogenic events. Senescent cells display a repressive chromatin configuration thought to stably silence proliferation-promoting genes, while simultaneously activating an unusual form of immune surveillance involving a secretory program referred to as the senescence-associated secretory phenotype (SASP). Here we demonstrate that senescence also involves a global remodeling of the enhancer landscape with recruitment of the chromatin reader BRD4 to newly activated super-enhancers adjacent to key SASP genes. Transcriptional profiling and functional studies indicate that BRD4 is required for the SASP and downstream paracrine signaling. Consequently, BRD4 inhibition disrupts immune cell mediated targeting and elimination of premalignant senescent cells *in vitro* and in *vivo*. Our results identify a critical role for BRD4-bound super-enhancers in senescence immune surveillance and in the proper execution of a tumor-suppressive program.

Keywords

Oncogene-induced senescence; enhancers; BRD4; immune surveillance; SASP

[*]Corresponding Authors: Scott W. Lowe, 415 E 68th Street, Box373, New York, NY, 10065, USA. Phone: 646-888-3342; Fax: 646-888-3347; ; Email: lowes@mskcc.org; and Christopher R. Vakoc, Cold Spring Harbor Laboratory, One Bungtown Road, Cold Spring Harbor, NY 11724, USA. Phone: 516-367-5045; Fax: 516-367-8453; ; Email: vakoc@cshl.edu

[7]These authors contributed equally to this work

C.R. Vakoc has ownership interest in a patent related to BET inhibitor use in leukemia and is a consultant/advisory board member for Syros. No potential conflicts of interest were disclosed by the other authors.

Introduction

Cellular senescence is a cell cycle arrest program that limits proliferation of damaged cells and can be triggered in response to diverse forms of cellular stress ([1], [2]). Although, initially defined as a phenotype of cultured fibroblasts ([3]), cellular senescence appears to have a broad impact on human health and disease. For example, cellular senescence can restrict tumorigenesis ([4], [5]), modulate chemotherapy responses ([6], [7], [8]), and may exert a primordial role in wound healing, tissue remodeling and repair ([9], [10], [11], [12], [13]). Moreover, senescent cells have been observed in aged or damaged tissues ([14]) and can contribute to the decline of tissue regeneration capacity with age ([15], [16]). Accordingly, disruption of senescence regulators can promote cancer or impair wound healing, and the elimination of senescent cells from tissues can enhance lifespan in mice ([17], [18]).

Beyond the cell cycle arrest phenotype, senescent cells display marked changes in cell morphology, show increased senescence-associated β-galactosidase (SA-β-gal) activity, and undergo dramatic changes in higher-order chromatin organization that are associated with a distinct transcriptional profile ([2]). Mechanistically, the best-understood feature of cellular senescence is its stable cell cycle arrest program, which renders senescent cells insensitive to mitogenic stimuli and undoubtedly contributes to key senescence phenotypes ([2], [19]). This arrest program involves a complex interplay between the RB and p53 tumor suppressor pathways ([19]), and is accompanied by marked changes in the chromatin landscape involving the redistribution of cellular heterochromatin and leading to stable repression of cell cycle regulatory genes ([20], [21]). Such a potently repressive chromatin environment presumably buffers against the activation of proliferation genes in response to mitogenic cues.

Conversely, senescent cells activate the expression of genes known to influence the tissue microenvironment, including matrix remodeling enzymes, growth factors, and immune-modulatory cytokines ([22], [23]). As a consequence, senescent cells display qualitative and quantitative changes in their secretome, a feature collectively referred to as the senescence-associated secretory phenotype (SASP) ([24], [25]). This gene activation program is controlled in part by factors such as NF-κB ([26]), C/EBPβ ([27]), mTOR ([28], [29]), MacroH2A.1 ([30]), and GATA4 ([31]). Among their many functions, SASP proteins mobilize immune cells and modify their activities, for example, by recruiting natural killer (NK) cells or altering macrophage polarization to kill and/or engulf senescent cells ([9], [32], [33], [34]). These immune-modulatory activities may be important for the resolution of certain wound healing responses ([9], [10], [13]), and underlie a unique form of immune surveillance that can eliminate premalignant or malignant cells undergoing senescence *in vivo* ([33], [35], [36]).

As is clear from the above, the biological roles of senescence rely on gene *repression* and *activation* programs that substantially alter cell function and fate. In certain developmental and pathological contexts, such dramatic gene expression changes rely on dynamic remodeling of enhancer landscapes, regulatory regions that when activated induce gene expression and maintain downstream biological circuits. For example, in embryonic stem cells (ESCs), exceptionally large stretches of H3K27Ac-marked regulatory elements, termed super-enhancers (SEs), are associated with genes that play prominent roles in ESC self-renewal ([37], [38]). In other cell types, SEs can contribute to lineage- and cellular state-specific

transcription, for example, by sustaining the expression of the oncogene *MYC* in leukemia and some solid tumors ([37], [39]) or driving pro-inflammatory responses in endothelial cells ([40]). Importantly, transcription of SE-associated genes relies on dense accumulation of co-factors such as the bromo and extra terminal domain (BET) proteins and is highly sensitive to perturbations in co-factor binding ([39], [40]). BET proteins such as BRD4 bind to chromatin in a manner that can be disrupted with small molecule drugs and, as such, BET inhibitors are currently in development to suppress certain hyper-inflammatory diseases and cancer ([41], [42], [43]).

Studies to date have explored enhancer dynamics in ESC self-renewal, cell lineage specification, inflammation and pro-oncogenic contexts. Here, we examine whether enhancer dynamics contribute to oncogene-induced senescence (OIS), a potently tumor suppressive program that limits the expansion of premalignant cells ([5], [19]). Through genome-wide chromatin profiling, we find that H3K27Ac-enriched enhancers undergo global remodeling in senescence, with the appearance of new SEs adjacent to key SASP genes. We further show that genetic or pharmacological suppression of BRD4 collapses SASP gene expression and thereby prevents the proper immune targeting of senescent cells *in vitro* and *in vivo*. Our results establish that enhancer remodeling and BRD4 are required for senescence-associated immune surveillance and, consequently, for the proper execution of the tumor suppressive senescence program.

Results

Enhancers undergo global remodeling during oncogene-induced senescence

The mechanisms underlying the execution and maintenance of OIS have been best studied in human diploid fibroblasts ([2], [19], [20]). In this model, senescence is triggered by the introduction of oncogenic H-Ras^{V12}, which provokes a proliferative burst followed by induction of p53, p16^{Ink4a}, cell cycle exit, and the production of SA-β-gal and SASP ([19], [44]). Previous work using this model established the importance of heterochromatin formation and transcriptional repression in the senescence-associated cell cycle arrest program ([20], [21]), and contributed to the characterization of the SASP ([25]). To study enhancer biology during senescence, we transduced IMR90 normal human diploid lung fibroblasts with H-Ras^{V12} and allowed the cells to senescence. For comparison, we also generated parallel populations of proliferating IMR90 cells, and cells made quiescent by serum withdrawal. Importantly, while such quiescent cells can be triggered to re-enter the cell cycle upon serum addition, senescent cells cannot ([2]).

Following lysis of cross-linked proliferating, senescent, and quiescent IMR90 cells, the enhancer landscape was visualized using chromatin immunoprecipitation coupled with high-throughput sequencing (ChIP-Seq) using the histone modification H3K27Ac as a marker of active enhancers ([45]). This analysis identified a total of ~33,000 H3K27Ac detectable enhancers in proliferating, quiescent and senescent IMR90 cells (union enhancers) (Fig. 1A). Previous studies have documented distinct classes of enhancers termed super-enhancers (SEs), which accumulate disproportional levels of chromatin modifications and are associated with key cell identity genes ([38], [39]). By implementing the previous definition of SEs based on H3K27Ac ChIP-Seq profiling ([39]), we identified ~1,250 SEs present across

the three cell conditions and classified the remaining ~32,000 as typical enhancers (TEs) (Figs. 1B and 1C).

To reveal enhancer dynamics during OIS, we next compared the H3K27Ac levels at enhancers in senescent cells to those in proliferating cells. Based on a cut-off of two-fold H3K27Ac enrichment over the proliferating condition, our analysis called ~6,500 senescence-activated TEs and ~7,090 senescence-inactivated TEs (Fig. 1B; Supplementary Table S1A and S1B), as well as 198 senescence-activated SEs and 191 senescence-inactivated SEs (Fig. 1C; Supplementary Tables S1C and S1D), suggesting that over 40% of all enhancers in IMR90 cells are remodeled upon senescence. Interestingly, while the majority of the senescence-activated TEs and SEs displayed the H3K4Me1 mark in proliferating IMR90 cells (Figs. S1A and S1B), senescence was found to selectively remodel the active mark H3K27Ac in a manner that distinguished this condition from both proliferating and quiescent cells. In particular, H3K27Ac signals gained and lost in senescent cells were not similarly altered during quiescence (Figs. 1D and 1E), indicating that such global enhancer remodeling was specific to the senescence condition and not an indirect consequence of cell cycle arrest *per se*. H3K27Ac ChIP-Seq profiles of exemplary TEs and SEs specifically activated or inactivated during OIS are depicted in Figs. 1F–1I. Importantly, these results were reproducible across independent biological replicates (Supplementary Figs. S2A and S2B; top panels). Altogether, these analyses reveal a global remodeling of active enhancers upon induction of OIS that occurs in a manner that distinguishes senescent cells from proliferating and quiescent counterparts.

Senescence-activated super-enhancers correlate with the SASP transcriptional profile

To address the impact of enhancer remodeling observed during OIS on global gene expression changes, we next performed genome-wide transcriptome profiling in proliferating, quiescent and senescent IMR90 cells by RNA-Sequencing (RNA-Seq). Unsupervised hierarchical clustering analysis grouped proliferating and quiescent samples closely together and clearly segregated them from the senescent samples (Fig. 2A). Importantly, gene set enrichment analysis (GSEA) showed a highly significant correlation between enhancer activity and transcriptional levels of the associated genes for both senescence-activated and -inactivated TEs and SEs (Figs. 2B–2E; FDR q-values = 0.00). Consistent with the specificity of the global enhancer remodeling during senescence (see Fig. 1), GSEA failed to identify similar correlations between the senescence-associated enhancer changes and the transcriptional output of quiescent versus proliferating cells (Supplementary Figs. S3A–S3D).

We next used gene ontology (GO) analysis to gain insights into the biological processes controlled by both categories of enhancers remodeled during OIS. GO analysis of the genes associated with senescence-activated TEs indicated an enrichment of negative regulators of MAPK pathway and TLR signaling pathway (Fig. 2F and Supplementary Fig. S3E; top panel), which have been previously implicated in senescence ([46], [47]). On the other hand, TEs inactivated in senescent cells were linked to genes involved in telomere maintenance, chromosome localization and DNA strand elongation/replication categories (Fig. 2G and Supplementary Fig. S3E; bottom panel), consistent with the cell cycle arrest that

accompanies senescence ([19]). These genes included many E2F targets (Supplementary Fig. S3E; bottom panel and Supplementary Table S1B), which are silenced during OIS through repressive histone marks ([20, 21]). Interestingly, despite the fact that E2F target genes are commonly down regulated in both quiescence and senescence (Supplementary Figs. S3F and S3G), their associated TEs were only found substantially remodeled in senescent cells (Supplementary Figs. S3H and S3I; and exemplified by the enhancer of the E2F target gene *MCM6* shown in Fig. 1G). This result is consistent with the known resistance of senescent cells (compared to quiescent cells) to induce growth-promoting genes following a mitogenic stimulus ([2]) and suggests that senescence-specific enhancer inactivation contributes to, or is a prerequisite for, the stable repression of cell cycle genes.

Dramatic changes were also observed in the SE landscape of senescent cells, with a robust activation of SEs in senescent compared to quiescent cells (Supplementary Fig. S3J). GO analysis on genes associated with such senescence-activated SEs indicated an enrichment of factors having cytokine and growth factor activity including the well described SASP factors IL-1A, IL-1B, IL-8, INHBA and BMP2 (Fig. 2H and Supplementary Fig. S3K; refs. [24, 26]). In contrast, SEs inactivated in senescent cells were associated with genes related to DNA binding transcription factors (TF) and fibronectin binding categories (Fig. 2I; and Supplementary Fig. S3K), the latter process likely reflecting the well-established reduction in extracellular matrix production that accompanies senescence ([48]). Examples of enhancer-regulated genes selectively activated or inactivated in senescent cells are depicted as heat maps in Figs. 2J–M. Together, these results connect enhancer remodeling to discrete senescence-associated transcriptional profiles, and suggest that TE inactivation likely contributes to the cell cycle arrest, while SE activation might underlie the robust expression of SASP genes in senescent cells.

BRD4 is recruited to senescence-activated SEs associated with key SASP genes

One of the proteins that bind acetylated histones at enhancers and are enriched in SEs is the transcriptional co-activator BRD4, which couples enhancer remodeling to RNA Pol II elongation ([39]). To address changes in BRD4 occupancy during OIS, we next performed ChIP-Seq profiling for BRD4 in proliferating, quiescent and senescent IMR90 cells. Despite similar numbers of overall raw and mapped reads across all three conditions (see Supplementary Fig. S2C), BRD4 binding at H3K27Ac enhancer elements showed a progressive decline in signal strength from proliferating to quiescent to senescent cells (Fig. 3A). Although the reduced signal correlated with a decrease in total BRD4 protein in non-proliferating versus proliferating conditions (Fig. 3B), this may also reflect nuances of the ChIP-Seq assay in senescent cells, which is less sensitive owing to the global compaction of chromatin ([49]). Nevertheless, comparison of BRD4 occupancy at senescence-activated H3K27Ac enhancer elements in senescent versus proliferating cells (log2 fold change > 0.5) uncovered a robust and reproducible local enrichment of BRD4 at specific enhancer loci (see Supplementary Fig. S2A and S2B, bottom panels). In particular, 1,307 TEs and 37 SEs significantly gained BRD4 binding during the establishment of senescence (Figs. 3C and 3D; Supplementary Tables S2A and S2B), which will be referred to as BRD4-gained TEs and BRD4-gained SEs, respectively.

Notably, while the BRD4 gain at senescence-activated TEs occurred significantly in both quiescent and senescent cells, albeit with different magnitudes (Fig. 3E), the gain of BRD4 at SEs was highly specific to the senescent cell state (Fig. 3F). Interestingly, BRD4-gained SEs were adjacent to key SASP genes with described regulatory and/or effector functions including the cytokines *IL-1A*, *IL-1B*, *IL-8* and the matrix metalloproteases *MMP1* and *MMP10* (Figs. 3D and 3G; Supplementary Table S2B) ([24], [28]). Consistently, such SEs were associated with genes related to the inflammatory response and immune system phenotype GO categories (Fig. 3H) and were selectively induced in senescent cells when compared to both proliferating and quiescent cells (Figs. 3I and 3J; FDR = 0.00). Given that BRD4 also co-operates with sequence-specific TFs for regulation of target genes, we performed *de novo* motif analysis on the BRD4-gained SE regions and identified several TFs such as NF-κB, a bona-fide SASP regulator ([26]), as well as FOS and ELK1 (Fig. 3K), known to be activated by RAS/MAPK signaling ([50]). Interestingly, motif analysis of all senescence-activated SEs also predicted sites for SMAD3, C/EBPβ and GATA family of transcriptions factors (data not shown), previously linked to senescence ([31], [51], [52]). Altogether, these results demonstrate that OIS is accompanied by recruitment of BRD4 to a subset of senescence-activated SEs flanking key SASP genes, and suggest that the SASP program may be particularly sensitive to SE disruption by chromatin targeting drugs.

The bromodomain protein BRD4 is critical for SASP gene expression

Having identified BRD4 enrichment at SE elements during OIS, we next sought to determine the impact of this factor on the transcriptional output of senescent cells. To this end, we inhibited BRD4 using a validated miR30-based short hairpin RNA (shRNA; ref. [53]) or the small molecule BET inhibitor JQ1 ([42]) and performed RNA-Seq in proliferating, quiescent and senescent IMR90 cells. For comparison, we also examined transcriptional profiles of cells expressing an shRNA targeting the RELA/p65 subunit of NF-κB, a well-characterized SASP regulator ([26]). As additional controls, we inactivated classical tumor suppressor genes (TSGs) such as p53 and RB, known to direct the gene *repression* program leading to a permanent cell cycle arrest ([20]), as well as the cell cycle regulators p21 and p16 (*CDKN1A* and *CDKN2A*), which when inhibited in combination can bypass senescence in IMR90 cells ([49]). Collectively, we envisioned this panel of cell states would allow us to pinpoint direct and indirect regulators underlying distinct modules of the senescence transcriptional program.

Following RNA-Seq profiling, we first defined a senescence signature by identifying the top 100 induced and repressed genes in senescent cells compared to proliferating cells but not in quiescent cells (Supplementary Tables S3A–S3C). This signature is similar to that produced by our laboratory using microarray technology ([26], [49]) and to those in previously published reports ([54], [55]). Hierarchical clustering analysis using this senescence signature revealed that BRD4 knockdown cells cluster away from the TSG knockdowns and closely together with p65 knockdown samples (Fig. 4A). This indicates that BRD4 controls a transcriptional module similar to that controlled by NF-κB but distinct from the cell cycle arrest program controlled by p53, RB, p16 and p21. Importantly, JQ1-treated senescent samples also clustered closely with BRD4 knockdown (Fig. 4A), supporting a bromodomain-dependent

function of BRD4 in the regulation of gene expression programs during senescence, as previously described in other contexts ([39], [40]).

We next defined a BRD4 senescence signature by identifying senescence-induced genes that were significantly down regulated (two-fold cut-off; $p<0.005$) upon BRD4 knockdown in senescent cells (Supplementary Table S3D). Principal component analysis (PCA) of this gene signature across the entire set of samples revealed a close clustering of BRD4 and p65 inhibited senescent samples with proliferating cells and away from the remaining senescence conditions, further supporting the distinct transcriptional output of BRD4 during OIS (Fig. 4B). GO analysis on the BRD4 senescence signature indicated a significant enrichment for terms related to immune system/inflammation, NF-κB and Ras (Fig. 4C), which included key SASP factors such *IL-1A, IL-1B,* and *IL-8* (Supplementary Figs. S4A and S4B) and other genes herein found to gain distal SE activity and BRD4 binding during senescence (see Fig. 3I). In agreement, GSEA showed a significant enrichment of the BRD4 signature in genes associated with the BRD4-gained SEs (Fig. 4D; FDR = 0.00), supporting a mechanism of SE-mediated regulation of BRD4 targets during OIS. Despite sharing an overlapping transcriptional output (Figs. 4A and 4B), RNA-Seq profiling indicated that BRD4 regulates a larger set of genes than p65 during senescence (300 vs. 162) (Fig. 4E, and Supplementary Tables S3D–S3G). Subsequent qRT-PCR validation using two independent BRD4 shRNAs and JQ1 similarly showed that not all BRD4-dependent SASP factors are NF-κB targets, which include, among others, INHBA, BMP2, VEGFA and VEGFC (Figs. 4F and 4G; and Supplementary Figs. S4C and S4D). These data indicate that BRD4 is major SASP regulator during OIS.

To determine whether these phenomena were restricted to OIS in IMR90 cells, we assessed whether SASP expression also depends on BRD4 in different cells lines and/or by different senescence triggers. BJ human foreskin fibroblasts and WI-38 human diploid lung fibroblasts triggered to senescence by oncogenic H-Ras^{V12} also showed that the classical SASP factors IL-1A, IL-1B, IL-6, IL-8, CXCL1 and MMP10 were induced in both cell types, and that this induction was blunted in cells harboring BRD4 shRNAs or treated with JQ1 (Supplementary Figs. S4E and S4F). Furthermore, IMR90 cells triggered to senescence by treatment with the topoisomerase inhibitor etoposide ([6], [7]) displayed similar changes in the enhancer landscape as occurred during OIS (Fig. 4H, and Supplementary Figs. S5A and S5B). However, the gain in H3K27Ac signal intensity adjacent to SASP genes was less than observed during OIS (Fig. 4H and Supplementary Fig. S5B), consistent with the lesser induction of SASP genes in this context (compare Figs. 4F and 4I, respectively). Still, genetic inactivation of BRD4 also blunted SASP gene expression in etoposide treated cells (Fig. 4I and Supplementary Fig. S5C). Of note, in both etoposide-induced senescence and OIS, JQ1 treatment blunted SASP even after cells had established senescence (Figs. 4F, 4G and 4I; and Supplementary Figs. S4B-S4F and S5C), suggesting a key role for BRD4 in the maintenance of this senescence program. Altogether, these results suggest that senescence-induced enhancer remodeling contributes broadly to senescence biology and establish BRD4-bound SEs as a critical regulator of the SASP that can be disrupted pharmacologically.

BRD4 is needed for acquisition of the senescence-associated secretome

Given this unexpected association between BRD4 and senescence, we explored the impact of BRD4 inhibition on a variety of senescent phenotypes. BRD4 suppression in the IMR90 Ras model did not result in significant changes in TSG activation (Fig. 5A), or in other senescence markers such as senescence-associated beta-galactosidase (SA-β-gal) activity (Fig. 5B), BrdU incorporation (Fig. 5C) or senescence-associated heterochromatin formation (SAHF; Fig. 5D). Colony formation at low cell density over two weeks was also not affected by BRD4 inhibition (Fig. 5E), further supporting that BRD4 inactivation does not bypass the senescence-associated cell cycle arrest. These findings contrast with the phenotypes observed following suppression of RB and p53 pathway components on cellular senescence and are consistent with the distinct impact of BRD4 knockdown on the transcriptional profiles of senescent cells (see Fig. 4A). To examine the impact of BRD4 suppression on the ultimate readout of SASP, we next examined a subset of the senescent cell secretome using commercially available cytokine arrays. Using this approach, we detected a clear accumulation of secreted G-CSF, GM-CSF, CXCL1, IL6, IL8 and MIF in the conditioned media (CM) from senescent cells when compared to proliferating cells. CM from senescent cells upon BRD4 knockdown, however, showed a clear reduction in the levels of these cytokines, showing that BRD4 inactivation affects the secretome of senescent cells (Figs. 5F and 5G). Collectively, these data indicate that BRD4 suppression selectively inhibits SASP but not other senescent phenotypes.

BRD4 is required for SASP-mediated paracrine signaling functions in vitro

The SASP transcriptional module produces marked changes in the secretome, which sends signals that influence the fate and function of neighboring cells within the tissue microenvironment ([2], [14]). Having identified BRD4 as a factor linking remodeling of the enhancer landscape and transcription program leading to SASP, we next examined its ability to influence the behavior of other cell types in a series of *in vitro* assays. First, we examined the ability of BRD4 to impact paracrine senescence, a phenomenon whereby CM from senescent cells can transmit senescence signals to naïve cells ([56], [57]). Treatment of naïve proliferating IMR90 cells with CM from senescent IMR90 cells inhibited proliferation (Fig. 6A) and induced SA-β-gal activity (Figs. 6B and 6C), effects that were impaired when naïve cells were treated with CM from BRD4-inhibited senescent cells (Figs. 6A–6C). Furthermore, the ability of CM from senescent cells to induce SASP factors such as IL-1A, IL-1B, IL-6 and IL-8 in proliferating cultures was also attenuated when using CM from senescent cells lacking BRD4 (Fig. 6D). Therefore, BRD4 is required for paracrine senescence, an effect that might amplify the impact of senescent cells in tissues.

We also examined the impact of BRD4 on the ability of senescent cells to modulate immune cell function and facilitate senescent cell targeting ([26], [33]). We previously showed that murine hepatic stellate cells undergoing senescence produce factors that could promote an anti-tumor M1 polarization of macrophages and recruit NK cells leading to senescent cell elimination ([9], [33]). To study the impact of fibroblasts undergoing OIS on macrophage polarization, we generated human monocyte-derived macrophages and treated them with CM from IMR90 cells that were proliferating or triggered to senesce by oncogenic Ras. Strikingly, CM from senescent cells produced a substantial increase in the M1 polarization

markers IL-1A, IL-1B, IL-6 and CCR7 in human macrophages, an effect that was substantially reduced when CM was prepared from senescent cells expressing BRD4 shRNAs (Fig. 6E, left panels). Markers associated with M2 polarization were unaffected under all conditions (Fig. 6E, right panels). To study NK cell-mediated cytotoxicity triggered by SASP, we co-cultured the YT human NK cell line with GFP-labeled proliferating or senescent IMR90 cells and observed a significant reduction of viable senescent cells when compared to proliferating counterparts ([9], [26]). Importantly, this NK-mediated cytotoxicity was significantly reduced when NK cells were co-cultured with BRD4-supressed senescent cells (Figs. 6F–6H; and Supplementary Movies S1–S3). Therefore, BRD4 is required for key components of the immune surveillance mechanisms that trigger the clearance of senescent cells.

Brd4 inhibition impairs immune surveillance of oncogenic N-Ras expressing senescent cells in vivo

The data presented above link SE remodeling and the emergence of SASP during senescence via BRD4, and imply that this factor ultimately contributes to the immune-modulatory and immune surveillance functions of the senescence program. To examine this in a physiologically relevant context, we took advantage of a powerful mouse model of OIS *in vivo*, where the induction of senescence can be acutely triggered and the fate of senescent cells can be monitored over time ([36]). In this model, sleeping beauty (SB) transposase and a SB transposon vector expressing oncogenic N-Ras are co-delivered into the tail vein of mice via hydrodynamic injection, a procedure that results in stable integration of the transposon selectively into hepatocytes. Oncogenic N-Ras rapidly triggers senescence and SASP, which in turn activate mechanisms of immune-mediated surveillance and clearance ([36]). We further adapted this model to co-express an N-Ras^{G12D}-IRES-GFP cassette and an shRNA targeting any gene in the same cells by co-delivering two functionally-linked transposon vectors: one in which N-Ras^{G12D} is regulated from a tetracycline responsive promoter and the other constitutively expressing the reverse tet-transactivator protein (rtTA) together with a miR30-based shRNA (Fig. 7A). We reasoned this system would enable tracing oncogene expressing cells using the linked GFP reporter and assessment of both pharmacological (systemic) and genetic (hepatocyte-specific) inhibition of Brd4 on senescent cell targeting and clearance *in vivo*.

We first assessed the impact of systemic Brd4 inhibition using the BET inhibitor I-BET762 (iBET), a compound analogous to JQ1 but with improved pharmacologic properties *in vivo* ([41]). Cohorts of mice that had been transduced with N-Ras^{G12D}-IRES-GFP and a neutral shRNA (shRen) were treated daily with iBET or vehicle (Fig. 7B), and livers analyzed for GFP-expressing senescent cells and immune cell infiltration at 6 and 12 days post-transduction. As shown in Fig. 7C (left panels) and 7D, both iBET and vehicle treated mice showed a similarly large fraction of GFP-positive cells at 6 days, indicating effective delivery of the transposon vectors. By day 12, livers isolated from vehicle treated mice showed a dramatic reduction in GFP-positive hepatocytes (Figs. 7C, top middle panel; and 7D), consistent with their immune-mediated clearance ([36]), and clusters of immune cells in close proximity to the remaining GFP-positive foci (Figs. 7C, top right panel; and 7E, top panel). By stark contrast, livers from iBET treated mice retained significantly more GFP-

positive foci (Figs. 7C, bottom middle panel and 7D). Importantly, although these foci were still SA-β-gal-positive (Supplementary Fig. S6A), they lacked the prominent immune cell infiltration observed in the livers of vehicle-treated animals (Figs. 7C, right panels; 7E and Supplementary Fig. S6B). Thus, pharmacological inhibition of the BET protein family clearly impairs senescence immune surveillance in this model.

Besides their novel role in senescence surveillance described above, BET proteins are crucial for the inflammatory response of various immune cells ([41], [58]). Since systematic iBET administration inhibits BET protein function in all cell types, it remains possible that the impaired senescence surveillance noted in iBET treated animals could arise through compromised immune cell function. To address this issue, we took advantage of our genetic model to selectively suppress Brd4 in oncogene-expressing hepatocytes (see Fig. 7A). Specifically, we injected mice with shRNAs targeting a neutral gene (shRen) or Brd4 (shBrd4-1; shBrd4-2), treated the mice with doxycycline, and monitored GFP-positive foci and immune cell infiltration as above.

The results from these experiments decisively showed that genetic inhibition of Brd4 in oncogene-expressing hepatocytes is sufficient to impair their proper immune surveillance. Hence, livers from mice transduced with a control shRNA showed abundant clearance of GFP-positive cells between day 6 and day 12 post-transfection, which was significantly impaired in livers from mice transduced with two independent Brd4 shRNAs (Figs. 7F and 7G). As was noted following pharmacological BET inhibition, this impaired clearance was not due to a failure to activate the senescence program (Supplementary Fig. S6C) but instead was associated with reduced immune cell infiltration (Figs. 7H–7J) and a blunted SASP response, as illustrated by the decreased levels of the chemokine Mcp1 (Ccl2) (Fig. 7K), previously implicated in this model ([36]). All together, these data indicate that Brd4 plays a key role in the immune-mediated clearance of oncogene expressing senescent cells *in vivo,* demonstrating its requirement for the full execution of the SASP-mediated tumor suppressive program.

Discussion

Cellular senescence occurs through a two-component process that leads to a stable cell cycle arrest and the activation of an immune-modulatory program that collectively limits cell expansion. The senescence-induced cell cycle program involves vast changes in the heterochromatin organization leading to transcriptional repression ([20], [21]), whereas the gene activation program can involve recruitment of key transcriptional activators ([31], [40], [59]). Here we demonstrate that each component of the senescence program is dictated by distinct changes in the enhancer landscape – on one hand, loss of TEs adjacent to the promoters of proliferation genes and, on the other, the acquisition of SEs flanking SASP genes leading to a BRD4-controled gene activation program. As a consequence of the latter program, BRD4 inhibition in pre-malignant senescent cells leads to a diminished SASP response and a compromised immune surveillance both *in vitro* and *in vivo*. These studies extend the role of BRD4-bound SEs in cancer beyond the establishment of tumor-promoting transcriptional circuits to a tumor suppressive program that stimulates the clearance of premalignant senescent cells.

The senescence-associated transcriptional profile is shaped by enhancer remodeling

Cellular identity and plasticity rely on dynamic remodeling of enhancer landscapes ([60]). By comparing the active enhancer landscape during OIS to proliferative and quiescent conditions, we uncovered a global enhancer remodeling process that drives the gene expression program linked to senescence. Hence, the acquisition and loss of enhancer activity at particular loci correlated well with gene expression patterns previously implicated in senescence ([46], [47], [48]). Of note, while repression of E2F target genes was similarly observed in both quiescent and senescent cells, the TEs associated with these loci were exclusively inactivated during senescence. This result is particularly intriguing as it likely underlies the epigenetic mechanism of the stable cell cycle arrest exhibited by senescent cells.

Most interestingly, SE activation resulted in induction of genes related to cytokine and growth factor activity, which include essential components of the SASP ([24], [26]) and also categorically distinguished senescent cells from growth-arrest quiescent counterparts. Interestingly, the SASP-associated SE loci that became activated during senescence displayed abundant H3K4Me1 marks in proliferating IMR90 cells, suggesting that they already pre-exist in inactive configurations (“primed”) in basal conditions and only gain the activating H3K27Ac mark upon Ras stimulation. This situation contrasts with that of macrophage activation in which a sub-set of enhancers are newly configured (“latent”) following a pro-inflammatory stimulus ([61]), Nevertheless, given the prominence of SEs in controlling cell identify and fate ([37], [38]), these observations underscore the importance of SASP as a key output of the senescence program.

Super-enhancer-associated BRD4 is required for SASP

SEs frequently associate with transcriptional co-regulators such as BET proteins to regulate gene expression ([37], [38]) and as such, SE-regulated genes are often highly sensitive to perturbation using BET inhibitors ([39], [40]). Indeed, using genome wide chromatin profiling, we observed that BRD4 is recruited to a subset of SEs associated with SASP genes during senescence, and that genetic or pharmacological inhibition of BRD4 collapses the senescence-induced SASP transcriptional program. Interestingly, while only a subset of SASP-associated enhancer loci gained substantial H3K27Ac mark and BRD4 binding during OIS, our RNA-Seq analysis indicated a high number of SASP genes that were repressed by BRD4 inactivation. In principle, this observation may reflect the reduced sensitivity of the ChIP-Seq assay in senescent cells. Alternatively, senescence-activated SEs may selectively trigger the expression of a specific class of SASP genes with key regulatory functions. For example, IL-1A and IL–1B, which are induced more than one thousand-fold through BRD4-gained SEs in senescence, are known SASP “amplifiers” ([27], [28], [52], [57], [62]) and, as such, could induce additional SASP factors through positive feedback loops without the need for direct BRD4 regulation. Consistent with this view, control of such amplifier genes may underlie the action of GATA4 on SASP during replicative senescence ([31]). Regardless, our findings establish BRD4-gained SEs as key players in the regulation of cellular senescence, unraveling novel regulatory nodes in senescent cells that can be targeted pharmacologically.

Besides binding acetylated histones that display an increase at senescence-activated SEs, the mechanism whereby BRD4 leads to transcriptional activation of SASP genes likely involves recruitment of specific TFs as described in others contexts ([63], [64], [65]). One of the TFs with consensus binding sites that were enriched in regions of senescence-activated SEs is NF-κB, which is reminiscent of observations during the inflammatory response of macrophages and endothelial cells ([40], [66]). Importantly, however, our results clearly show that BRD4 can control non-NF-κB targets involved in SASP, suggesting it has non-redundant functions with NF-κB during senescence. It is likely that multiple TFs orchestrate the impact of BRD4-gained SEs on SASP gene transcription including FOS, ELK1, PRDM19 and others besides NF-κB as indicated by our motif analysis. Moreover, analyses of all H3K27Ac-marked SEs identified additional TF such as SMAD3, C/EBPβ or the GATA family, previously linked to senescence ([31], [51], [52]) as well as to liver fibrosis ([67]), pointing to both specific and common regulatory mechanisms driving enhancer-mediated secretory pathway activation in different cellular contexts.

Our results also provide new insights into the diametrically opposed epigenetic mechanisms coordinating different components of the senescence program. Previous studies documented the importance of heterochromatin reorganization together with the recruitment of histone-modifying enzymes for the production of a repressive chromatin environment on the promoters of cell cycle genes ([20], [21]). As shown here, these genes are often governed by TEs in proliferating cells that are inactivated during OIS and are not dependent on BRD4. By stark contrast, the gene activation program associated with SASP is ultimately directed by a redistribution of BRD4 within senescence-activated SEs associated with key SASP regulators. Importantly, as a consequence of the exquisite sensitivity of SE-regulated transcription to BET inhibition, genetic and pharmacologic inhibition of BRD4 collapses the SASP signature and diminishes SASP-mediated functions *in vitro* and *in vivo* while having no impact on the senescence-associated cell cycle arrest. Thus, these results indicate that BRD4 inactivation uncouples the SASP from the cell cycle arrest during senescence, and imply that BET inhibitors may be valuable at modulating SASP activity *in vivo*, such as has been recently reported for the mTOR inhibitor rapamycin ([28], [29]).

BRD4 is required for paracrine senescence and immune surveillance

BET protein-associated SEs are important in establishing biological circuits in cancer and other processes, such as ESC self-renewal, cell lineage specification and inflammation ([37], [38], [39], [40]). In contrast, our study links SE remodeling to senescence immune surveillance and, in doing so, reveals an unexpected role for BRD4 in the tumor suppressive senescence program. Specifically, we show that BRD4, while being dispensable for the senescence-associated cell cycle arrest, is critical for paracrine senescence transmission, macrophage M1 polarization, and senescent-cell targeting by NK cells. More importantly, using a mouse model of senescence immune surveillance in the liver, we demonstrate that Brd4 inhibition *in vivo* disrupts SASP gene expression and the efficient clearance of pre-malignant senescent hepatocytes. Collectively, these results suggest that BRD4 is a master regulator that controls senescent cell communication with the microenvironment.

Our data linking BRD4 to a tumor suppressive program stands in apparent contrast to the established role of BRD4 in tumors as a cancer maintenance gene ([39], [53], [68]). Still, consistent with a potential role for BRD4 in other tumor suppressive programs, BRD4 inhibition can enhance oncogenic dedifferentiation in human breast cancer cells and cells from premature aging syndrome patients ([69], [70]), and promotes hyperproliferation in the murine epidermis ([71]). Moreover, although BRD4 had no marked impact on p53 transcriptional profiles in our system, phosphorylated BRD4 can act as a transcriptional co-activator for p53 in certain cell types ([72]). In principle, the impaired SASP response produced by sustained BRD4 inhibition might enable rare oncogene-expressing cells to eventually evade senescence and progress to cancer. Consistent with this possibility, we observed an aggressive hepatocellular carcinoma in one out of ten mice co-transduced with N-Ras^{G12D} and Brd4 shRNAs one year following liver transduction, while no tumors were observed in a similar number of mice transduced with N-Ras^{G12D} and a control shRNA (data not shown). In any event, our data support the view that BRD4 function is context-specific and, as such, the impact of BET inhibition may have markedly different consequences depending on cell lineage or genotype. Thus, while BET inhibitors may have anti-cancer effects owing to their ability to block aberrant cell renewal, they may simultaneously disrupt immune cell function or immune surveillance and, as such, their clinical impact will be determined by the balance of these effects.

Our results establish a key mechanism underlying the regulation of SASP gene expression that is responsible for the communication between cells undergoing OIS and the tissue microenvironment. Moreover, they begin to unravel the molecular framework of an immune surveillance network that, while understudied, might eventually be harnessed to engage the innate immune system for cancer therapy in a manner that complements current efforts to reawaken the adaptive immune system in cancer patients. Besides its role in cancer, the SASP response also contributes to tissue repair ([10], [13]), fibrosis ([9], [66]) and aging ([73]) and, in principle, BET inhibitors could provide strategies to modulate the SASP response and these processes at the organismal level.

Methods

Cell culture and retroviral infection

Human diploid IMR90, WI38 lung fibroblasts and human BJ foreskin fibroblasts were obtained from the American Type Culture Collection (ATCC), where they had been authenticated by short tandem repeat (STR) profiling, and were cultured in DMEM supplemented with 10 % fetal bovine serum (FBS) and penicillin and streptomycin (GIBCO). Frozen stocks generated within 2–3 passages from date of purchase were used throughout the study. Human macrophages were generated from monocytes isolated from buffy coats from healthy human blood donors (New York Blood Center) and differentiated in Teflon-coated cell culture bags in the presence of human CSF-1 (R&D Systems), as previously described ([74]). Resulting human monocyte-derived macrophages were cultured in RPMI-1640 with 2 % human serum (Sigma) and penicillin and streptomycin (GIBCO). Natural killer (NK) cells (from DSMZ; ref. [26]) were cultured in RPMI-1640 with 10 % FBS. For retroviral-mediated gene transduction, retroviruses were packed using Phoenix

cells (G. Nolan, Stanford University, CA) and infections were performed as described elsewhere ([20]). The infected population was selected using 2 μg/mL puromycin (Sigma) and 75 μg/mL hygromycin B (Roche). For JQ1 treatments, cells were treated with 100 nM of JQ1 or DMSO as vehicle for 48 hours (hr) prior to harvest. A working solution of JQ1 at 1 mM was prepared to use a final concentration of vehicle (DMSO) no higher than 1/10000.

Induction of senescence and quiescence

Senescence was induced in human cells by treatment with etoposide (100 μM; Sigma) for 2 days, or by retroviral-mediated expression of H-Ras^{V12}, as previously described ([20]). Vehicle-treated cells, or cells transduced with empty vector served as proliferating counterpart controls, respectively. When indicated, cells were co-transduced with vectors encoding validated GFP-linked shRNAs targeting BRD4 ([53]), p65 ([26]), p53 ([33]), p53/Rb ([49]), or p21/p16 ([49]). Infected cells were harvested 12 days post-infection. Quiescence was induced by culturing IMR90 cells in 0.1 % FBS for 4 days.

Senescence in vitro assays

BrdU incorporation, colony formation and senescence-associated-β-galactosidase (SA-β-gal) assays in cells were performed as previously described ([20, 26]). Briefly, senescent IMR90 cells (post-selection day 8) were plated on coverslips coated with 0.1 % gelatin and fixed in 4 % formaldehyde. For cell cycle arrest analyses, cells were labeled with BrdU (100 μg/mL; Sigma) for 6 hr and nuclei incorporating BrdU were visualized by immunolabeling with anti-BrdU antibodies (1:400; BD Pharmingen) as described previously ([20]). For colony formation assays, 1250, 2500, or 5000 cells were plated in each well of a six-well plate. Cells were cultured for 14 days, then fixed with 4 % formaldehyde and stained with crystal violet. Detection of SA-β-gal activity in mouse tissues was performed as described ([26]). For macrophage polarization experiments, 48 hr-conditioned media (CM) (containing FBS) was collected from proliferating (IMR90-vector) or senescent (IMR90-H-Ras^{V12}) cells expressing the indicated shRNAs, and seeded at day 6 post-pWZL-Hygro/shRNA transduction to have equal final cell numbers. CM was clarified by centrifugation, filtered through a 0.45 μm filter, diluted 1:3 with human monocyte-derived macrophage media and added to 500,000 human monocyte-derived macrophages, seeded in 6-well plates 24 hr before. Human macrophages were harvested following an 18 hr-incubation with the indicated CM and processed for qRT-PCR analysis of previously described M1 or M2 polarization markers ([75, 76]). NK cell cytotoxicity experiments were performed as described elsewhere ([26, 33]) with the following variations: NK cells were first stained with the CellTracker Red CMTPX Dye (Thermo Fisher Scientific) according to the manufacturer's instructions, briefly cell staining was performed in RPMI supplemented with 10 % FBS for 30 min using a final concentration of 1 μM of CellTracker Red CMTPX Dye, and then washed twice with PBS. NK cells were then seeded into 96-wells containing proliferating or senescent IMR90 cells expressing the indicated GFP-linked shRNAs. Co-cultures were imaged over time using an INCell 6000 high-content imager (GE Healthcare Life Sciences), with the 488 nm and 561 nm laser excitation, using a 10 X objective. The correct focal plane was maintained by the use of the INCell laser based focus system at each time point, which maintains a focal plane relative to the bottom of the well. Images were captured every 30 minutes in a temperature-controlled incubation chamber, starting 30

minutes after NK cell seeding onto IMR90 cultures. Cells were maintained in CO2 independent media (Life Technologies). Images for each channel were saved during the experiment and subsequently analyzed using GE Developer image analysis software (GE Healthcare Life Sciences). GFP labeled IMR90 cells were identified and segmented from background using an intensity-based threshold method. Touching cells and clumps of cells were segmented using watershed segmentation. NK cells labeled with the CellTracker Red CMTPX Dye were identified using the same threshold and segmentation method as the IMR90 cells. The average area of the GFP-labeled IMR90 cells was used as a measure of cell health and viability. The association of NK cells with IMR90 cells was quantified by measuring the fraction of the IMR90 cell area per well, overlapped with the total NK cell area per well. This value was normalized to the total area of GFP positive IMR90 cells per well. Paracrine senescence assays were performed as previously described ([57]). In brief, conditioned media (CM) was harvested from 2×10^6 (in a 10-cm dish) IMR90-vector proliferating cells or IMR90-H-Ras^{V12} senescent cells plated at day 10 post-infection and incubated in DMEM 0.5 % FBS for 72 hr. CM was clarified by centrifugation, filtered through a 0.45 μm filter and mixed with DMEM 40 % FBS in a proportion of 3 to 1 to generate CM containing 10% FBS. Cells were fixed for SA-βgal staining after 7 days and collected for RNA extraction 5 days after incubation; fresh media was added on top on day 3. All experiments were performed with biological duplicates and were repeated at least twice.

ChIP-Seq and bioinformatics analysis

ChIP-Seq was performed as previously described ([65]). H3K27Ac and H3K4Me1 antibodies were purchased from Abcam (ab4729 and ab8895, respectively). BRD4 antibody used for ChIP-Seq was purchased from Bethyl (A301-985A100). 0.5-1.0 ug of each antibody per 0.5 – 1.0 million cells was used. ChIP-Seq libraries were constructed using TruSeq ChIP Sample Prep Kit (Illumina) and sequenced using an Illumina HiSeq 2000 platform. Raw reads were mapped to the reference human genome assembly GRCh37 (hg19) using Bowtie and SAMtools. GREAT tool was used to predict GO terms of ChIP-Seq enriched regions ([77]). Gene set enrichment analyses (GSEA) were performed according to the instructions. Motif enrichment was identified with 1,000-bp window centered on 37 BRD4-associated enhancers using HOMER suite. Further details can be found in Supplementary Methods. The GEO accession number for the raw and processed ChIP-Seq data reported in this paper is GSE74238.

Identifying of senescence-activated H3K27Ac-enriched enhancers

Peaks from all conditioned H3K27Ac ChIP-Seq samples were combined first. After stitching regions with a maximum distance of 12.5-Kb, 31,731 H3K27Ac typical-enhancers and 1,255 H3K27Ac super-enhancers were identified (total union enhancers are 32,986). If the log2 fold changes of senescent versus proliferating was greater or less than two, they were assigned as senescence-activated or -inactivated enhancers, respectively. Using this approach, 6,555 senescence-activated and 7,095 senescence-inactivated typical-enhancers were defined from 31,731 typical-enhancers. Similarly, 198 senescence-activated and 191 senescence-inactivated super-enhancers were defined from 1,255 super-enhancers.

Identification of BRD4-gained senescence-activated super-enhancers

BRD4 tag counts were calculated from 4,440 and 198 senescence-activated typical- or super-enhancers, respectively. BRD4-gained enhancers were defined if log2 fold changes of BRD4 signals of senescence condition versus proliferating condition were greater than 0.5. With this criterion, 1,307 and 37 BRD4-gained typical- and super-enhancers were identified, respectively.

Expression analyses

Total RNA was isolated using the RNeasy minikit (Qiagen), and cDNA was obtained using the TaqMan reverse transcription reagents (Applied Biosystems). qRT-PCR data analyses were performed as previously described ([26]). Details of qRT-PCR, RNA sequencing (RNA-Seq), cytokine arrays, protein immunoblotting in cultured cells, and histological analyses in tissue sections are also provided in Supplementary Methods. The GEO accession number for the raw and processed RNA-Seq data reported in this paper is GSE74324.

In vivo senescence surveillance assays upon systemic or hepatocyte-specific Brd4 inhibition

For induction of OIS *in vivo*, sleeping beauty (SB) transposase vector and two SB transposon vectors expressing N-Ras^{G12D}-IRES-GFP and a miR30-shRNA (against Renilla or Brd4; see Supplementary Methods for additional details) were co-delivered into C57BL/6J mice (purchased from Harlan-Teklad) via hydrodynamic injection. Mice were injected with a sterile 0.9 % NaCl solution of 12.5 μg DNA of each transposon vector together with CMV-SB13 Transposase (1:5 ratio) via the lateral tail vein. Doxycycline was administered to mice via 625 mg/kg doxycycline-containing food pellets (Harlan Teklad), starting 24 hr before injections. For pharmacologic inhibition of Brd4, i-BET-762 (Selleck Chemicals) was reconstituted in dimethylsulfoxide (DMSO) and further diluted in phosphate-buffered saline (PBS). Mice were treated with I-BET 762 or vehicle orally every day (15mg/kg). Mice were sacrificed at the indicated time points and chunks of liver tissue with either fixed in 10% neutral buffered formalin or fresh frozen in Optimal Cutting Temperature (OCT) compound for histological analyses performed as detailed in Supplementary Methods. All experiments with mice were performed in accordance with protocols approved by the Memorial Sloan-Kettering Cancer Center's Internal Animal Care and Use Committee (IACUC) and Federal Office of Laboratory Animal Welfare guidelines.

Statistical analysis

Statistical tests performed to assess the significance of the Chip-Seq, RNA-Seq, qRT-PCR, histological, and functional data indicated above are described in Supplementary Methods.

Supplementary Material

Refer to Web version on PubMed Central for supplementary material.

Acknowledgments

Financial Support: This study was supported by funds from an RO1 grant (AG16379) from the NIH to S.W.L, CA013106 and the NIH/NCI Cancer Center Support Grant P30 CA008748. N.T. was supported by Lindsay and

Goldberg Fellowship from Watson School of Biological Sciences. A.B. was supported by an EMBO long-term fellowship. D.A.C. is recipient of a postdoctoral fellowship from the Spanish Fundación Ramón Areces. J.S.R. is supported by the Martin Sass Foundation and the Lauri Strauss Leukemia Foundation. S.W.L is an investigator in the Howard Hughes Medical Institute and the Geoffrey Beene Chair of Cancer Biology.

The authors gratefully acknowledge Sha Tian, John P. Morris IV, Leila Akkari, Florian Klemm, Johanna Joyce, Valery Krizhanovsky, Lars Zender, Amaia Lujambio for expert technical assistance and advice, Jonathan Brown, Charles Lin and Jay Bradner for key insights and technical advice, members of the Lowe laboratory and Charles J. Sherr for helpful comments.

Abbreviations

OIS	Oncogene-induced senescence
SEs	Super-enhancers
TEs	Typical enhancers
SASP	Senescence-associated secretory phenotype
BET	Bromo and extra terminal domain
SA-β-gal	Senescence-associated β-galactosidase activity
ChIP	Chromatin immunoprecipitation
NK	Natural killer cells
GSEA	Gene set enrichment analysis
GO	Gene ontology
PCA	Principal component analysis
TSGs	Tumor suppressor genes
SAHFs	Senescence associated-heterochromatic foci
CM	Conditioned media
SB	Sleeping-beauty
shRNA	transposase, small hairpin RNA

References

1. Collado M, Blasco MA, Serrano M. Cellular senescence in cancer and aging. Cell. 2007; 130:223–33. [PubMed: 17662938]
2. Kuilman T, Michaloglou C, Mooi WJ, Peeper DS. The essence of senescence. Genes Dev. 2010; 24:2463–79. [PubMed: 21078816]
3. Hayflick L, Moorhead PS. The serial cultivation of human diploid cell strains. Exp Cell Res. 1961; 25:585–621. [PubMed: 13905658]
4. Prieur A, Peeper DS. Cellular senescence in vivo: a barrier to tumorigenesis. Curr Opin Cell Biol. 2008; 20:150–5. [PubMed: 18353625]
5. Collado M, Serrano M. Senescence in tumours: evidence from mice and humans. Nat Rev Cancer. 2010; 10:51–7. [PubMed: 20029423]

6. te Poele RH, Okorokov AL, Jardine L, Cummings J, Joel SP. DNA damage is able to induce senescence in tumor cells in vitro and in vivo. Cancer Res. 2002; 62:1876–83. [PubMed: 11912168]
7. Roninson IB. Tumor cell senescence in cancer treatment. Cancer Res. 2003; 63:2705–15. [PubMed: 12782571]
8. Schmitt CA, Fridman JS, Yang M, Lee S, Baranov E, Hoffman RM, et al. A senescence program controlled by p53 and p16INK4a contributes to the outcome of cancer therapy. Cell. 2002; 109:335–46. [PubMed: 12015983]
9. Krizhanovsky V, Yon M, Dickins RA, Hearn S, Simon J, Miething C, et al. Senescence of activated stellate cells limits liver fibrosis. Cell. 2008; 134:657–67. [PubMed: 18724938]
10. Jun JI, Lau LF. The matricellular protein CCN1 induces fibroblast senescence and restricts fibrosis in cutaneous wound healing. Nat Cell Biol. 2010; 12:676–85. [PubMed: 20526329]
11. Muñoz-Espín D, Cañamero M, Maraver A, Gómez-López G, Contreras J, Murillo-Cuesta S, et al. Programmed cell senescence during mammalian embryonic development. Cell. 2013; 155:1104–18. [PubMed: 24238962]
12. Storer M, Mas A, Robert-Moreno A, Pecoraro M, Ortells MC, Di Giacomo V, et al. Senescence is a developmental mechanism that contributes to embryonic growth and patterning. Cell. 2013; 155:1119–30. [PubMed: 24238961]
13. Demaria M, Ohtani N, Youssef SA, Rodier F, Toussaint W, Mitchell JR, et al. An essential role for senescent cells in optimal wound healing through secretion of PDGF-AA. Dev Cell. 2014; 31:722–33. [PubMed: 25499914]
14. Muñoz-Espín D, Serrano M. Cellular senescence: from physiology to pathology. Nat Rev Mol Cell Biol. 2014; 15:482–96. [PubMed: 24954210]
15. Janzen V, Forkert R, Fleming HE, Saito Y, Waring MT, Dombkowski DM, et al. Stem cell ageing modified by the cyclin-dependent kinase inhibitor p16INK4a. Nature. 2006; 443:421–6. [PubMed: 16957735]
16. Burd CE, Sorrentino JA, Clark KS, Darr DB, Krishnamurthy J, Deal AM, et al. Monitoring tumorigenesis and senescence in vivo with a p16(INK4a)-luciferase model. Cell. 2013; 152:340–51. [PubMed: 23332765]
17. Baker DJ, Childs BG, Durik M, Wijers ME, Sieben CJ, Zhong J, et al. Naturally occurring p16(Ink4a)-positive cells shorten healthy lifespan. Nature. 2016; 530:184–9. [PubMed: 26840489]
18. van Deursen JM. The role of senescent cells in ageing. Nature. 2014; 509:439–46. [PubMed: 24848057]
19. Serrano M, Lin AW, McCurrach ME, Beach D, Lowe SW. Oncogenic ras provokes premature cell senescence associated with accumulation of p53 and p16INK4a. Cell. 1997; 88:593–602. [PubMed: 9054499]
20. Narita M, Nnez S, Heard E, Narita M, Lin AW, Hearn SA, et al. Rb-mediated heterochromatin formation and silencing of E2F target genes during cellular senescence. Cell. 2003; 113:703–16. [PubMed: 12809602]
21. Zhang R, Poustovoitov MV, Ye X, Santos HA, Chen W, Daganzo SM, et al. Formation of MacroH2A-containing senescence-associated heterochromatin foci and senescence driven by ASF1a and HIRA. Dev Cell. 2005; 8:19–30. [PubMed: 15621527]
22. Coppé JP, Desprez PY, Krtolica A, Campisi J. The senescence-associated secretory phenotype: the dark side of tumor suppression. Annu Rev Pathol. 2010; 5:99–118. [PubMed: 20078217]
23. Freund A, Orjalo AV, Desprez PY, Campisi J. Inflammatory networks during cellular senescence: causes and consequences. Trends Mol Med. 2010; 16:238–46. [PubMed: 20444648]
24. Coppé JP, Patil CK, Rodier F, Sun Y, Muñoz DP, Goldstein J, et al. Senescence-associated secretory phenotypes reveal cell-nonautonomous functions of oncogenic RAS and the p53 tumor suppressor. PLoS Biol. 2008; 6:2853–68. [PubMed: 19053174]
25. Kuilman T, Peeper DS. Senescence-messaging secretome: SMS-ing cellular stress. Nat Rev Cancer. 2009; 9:81–94. [PubMed: 19132009]
26. Chien Y, Scuoppo C, Wang X, Fang X, Balgley B, Bolden JE, et al. Control of the senescence-associated secretory phenotype by NF-κB promotes senescence and enhances chemosensitivity. Genes Dev. 2011; 25:2125–36. [PubMed: 21979375]

27. Kuilman T, Michaloglou C, Vredeveld LC, Douma S, van Doorn R, Desmet CJ, et al. Oncogene-induced senescence relayed by an interleukin-dependent inflammatory network. Cell. 2008; 133:1019–31. [PubMed: 18555778]
28. Laberge RM, Sun Y, Orjalo AV, Patil CK, Freund A, Zhou L, et al. MTOR regulates the pro-tumorigenic senescence-associated secretory phenotype by promoting IL1A translation. Nat Cell Biol. 2015; 17:1049–61. [PubMed: 26147250]
29. Herranz N, Gallage S, Mellone M, Wuestefeld T, Klotz S, Hanley CJ. mTOR regulates MAPKAPK2 translation to control the senescence-associated secretory phenotype. Nat Cell Biol. 2015; 17:1205–17. [PubMed: 26280535]
30. Chen H, Ruiz PD, McKimpson WM, Novikov L, Kitsis RN, Gamble MJ. MacroH2A1 and ATM Play Opposing Roles in Paracrine Senescence and the Senescence-Associated Secretory Phenotype. Mol Cell. 2015; 59:719–31. [PubMed: 26300260]
31. Kang C, Xu Q, Martin TD, Li MZ, Demaria M, Aron L, et al. The DNA damage response induces inflammation and senescence by inhibiting autophagy of GATA4. Science. 2015; 349:aaa5612. [PubMed: 26404840]
32. Iannello A, Thompson TW, Ardolino M, Lowe SW, Raulet DH. p53-dependent chemokine production by senescent tumor cells supports NKG2D-dependent tumor elimination by natural killer cells. J Exp Med. 2013; 210:2057–69. [PubMed: 24043758]
33. Lujambio A, Akkari L, Simon J, Grace D, Tschaharganeh FD, Bolden JE, et al. Non-cell-autonomous tumor suppression by p53. Cell. 2013; 153:449–60. [PubMed: 23562644]
34. Sagiv A, Biran A, Yon M, Simon J, Lowe SW, Krizhanovsky V. Granule exocytosis mediates immune surveillance of senescent cells. Oncogene. 2013; 32:1971–7. [PubMed: 22751116]
35. Xue W, Zender L, Miething C, Dickins RA, Hernando E, Krizhanovsky V, et al. Senescence and tumour clearance is triggered by p53 restoration in murine liver carcinomas. Nature. 2007; 445:656–60. [PubMed: 17251933]
36. Kang TW, Yevsa T, Woller N, Hoenicke L, Wuestefeld T, Dauch D, et al. Senescence surveillance of pre-malignant hepatocytes limits liver cancer development. Nature. 2011; 479:547–51. [PubMed: 22080947]
37. Hnisz D, Abraham BJ, Lee TI, Lau A, Saint-André V, Sigova AA, et al. Super-Enhancers in the Control of Cell Identity and Disease. Cell Resource. 2013; 155:934–47.
38. Whyte WA, Orlando DA, Hnisz D, Abraham BJ, Lin CY, Kagey MH, et al. Master transcription factors and mediator establish super-enhancers at key cell identity genes. Cell. 2013; 153:307–19. [PubMed: 23582322]
39. Lovén J, Hoke HA, Lin CY, Lau A, Orlando DA, Vakoc CR, et al. Selective inhibition of tumor oncogenes by disruption of super-enhancers. Cell. 2013; 153:320–34. [PubMed: 23582323]
40. Brown JD, Lin CY, Duan Q, Griffin G, Federation AJ, Paranal RM, et al. NF-κB Directs Dynamic Super Enhancer Formation in Inflammation and Atherogenesis. Mol Cell. 2014; 56:219–31. [PubMed: 25263595]
41. Nicodeme E, Jeffrey KL, Schaefer U, Beinke S, Dewell S, Chung CW, et al. Suppression of inflammation by a synthetic histone mimic. Nature. 2010; 468:1119–23. [PubMed: 21068722]
42. Filippakopoulos P, Qi J, Picaud S, Shen Y, Smith WB, Fedorov O, et al. Selective Filippakopoulos inhibition of BET bromodomains. Nature. 2010; 468:1067–73. [PubMed: 20871596]
43. Shi J, Vakoc CR. The Mechanisms behind the Therapeutic Activity of BET Bromodomain Inhibition. Mol Cell. 2014; 54:728–36. [PubMed: 24905006]
44. Courtois-Cox S, Jones SL, Cichowski K. Many roads lead to oncogene-induced senescence. Oncogene. 2008; 27:2801–9. [PubMed: 18193093]
45. Creyghton MP, Cheng AW, Welstead GG, Kooistra T, Carey BW, Steine EJ, et al. Histone H3K27ac separates active from poised enhancers and predicts developmental state. Proc Natl Acad Sci USA. 2010; 107:21931–6. [PubMed: 21106759]
46. Courtois-Cox S, Genther Williams SM, Reczek EE, Johnson BW, McGillicuddy LT, Johannessen CM, et al. A negative feedback signaling network underlies oncogene-induced senescence. Cancer Cell. 2006; 10:459–72. [PubMed: 17157787]

47. Olivieri F, Rippo MR, Prattichizzo F, Babini L, Graciotti L, Recchioni R, et al. Toll like receptor signaling in "inflammaging": microRNA as new players. Immun Ageing. 2013; 19:11. [PubMed: 23506673]
48. Shelton DN, Chang E, Whittier PS, Choi D, Funk WD. Microarray analysis of replicative senescence. Curr Biol. 1999; 9:939–45. [PubMed: 10508581]
49. Chicas A, Wang X, Zhang C, McCurrach M, Zhao Z, Mert O, et al. Dissecting the unique role of the retinoblastoma tumor suppressor during cellular senescence. Cancer Cell. 2010; 17:376–87. [PubMed: 20385362]
50. Gille H, Sharrocks AD, Shaw PE. Phosphorylation of transcription factor p62TCF by MAP kinase stimulates ternary complex formation at c-fos promoter. Nature. 1992; 358:414–7. [PubMed: 1322499]
51. Vijayachandra K, Lee J, Glick AB. Smad3 regulates senescence and malignant conversion in a mouse multistage skin carcinogenesis model. Cancer Res. 2003; 63:3447–52. [PubMed: 12839923]
52. Acosta JC, O'Loghlen A, Banito A, Guijarro MV, Augert A, Raguz S, et al. Chemokine signaling via the CXCR2 receptor reinforces senescence. Cell. 2008; 133:1006–18. [PubMed: 18555777]
53. Zuber J, Shi J, Wang E, Rappaport AR, Herrmann H, Sison EA, et al. RNAi screen identifies Brd4 as a therapeutic target in acute myeloid leukaemia. Nature. 2011; 478:524–8. [PubMed: 21814200]
54. Mason DX, Jackson TJ, Lin AW. Molecular signature of oncogenic ras-induced senescence. Oncogene. 2004; 23:9238–46. [PubMed: 15489886]
55. Fridman AL, Tainsky MA. Critical pathways in cellular senescence and immortalization revealed by gene expression profiling. Oncogene. 2008; 27:5975–87. [PubMed: 18711403]
56. Wajapeyee N, Serra RW, Zhu X, Mahalingam M, Green MR. Oncogenic BRAF induces senescence and apoptosis through pathways mediated by the secreted protein IGFBP7. Cell. 2008; 132:363–74. [PubMed: 18267069]
57. Acosta JC, Banito A, Wuestefeld T, Georgilis A, Janich P, Morton JP, et al. A complex secretory program orchestrated by the inflammasome controls paracrine senescence. Nature Cell Biology. 2013; 15:978–90. [PubMed: 23770676]
58. Belkina AC, Nikolajczyk BS, Denis GV. BET protein function is required for inflammation: Brd2 genetic disruption and BET inhibitor JQ1 impair mouse macrophage inflammatory responses. J Immunol. 2013; 190:3670–8. [PubMed: 23420887]
59. Capell BC, Drake AM, Zhu J, Shah PP, Dou Z, Dorsey J, et al. MLL1 is essential for the senescence- associated secretory phenotype. Genes Dev. 2016; 30:321–36. [PubMed: 26833731]
60. Shlyueva D, Stampfel G, Stark A. Transcriptional enhancers: from properties to genome-wide predictions. Nature Reviews Genetics. 2014; 15:272–86.
61. Ostuni R, Piccolo V, Barozzi I, Polletti S, Termanini A, Bonifacio S, et al. Latent enhancers activated by stimulation in differentiated cells. Cell. 2013; 152:157–71. [PubMed: 23332752]
62. Orjalo AV, Bhaumik D, Gengler BK, Scott GK, Campisi J. Cell surface-bound IL-1α is an upstream regulator of the senescence-associated IL-6/IL-8 cytokine network. Proc Natl Acad Sci USA. 2009; 106:17031–6. [PubMed: 19805069]
63. Shi J, Wang Y, Zeng L, Wu Y, Deng J, Zhang Q, et al. Disrupting the interaction of BRD4 with diacetylated Twist suppresses tumorigenesis in basal-like breast cancer. Cancer Cell. 2014; 25:210–25. [PubMed: 24525235]
64. Wu T, Pinto HB, Kamikawa YF, Donohoe ME. The BET family member BRD4 interacts with OCT4 and regulates pluripotency gene expression. Stem Cell Reports. 2015; 4:390–403. [PubMed: 25684227]
65. Roe JS, Mercan F, Rivera K, Pappin DJ, Vakoc CR. BET Bromodomain Inhibition Suppresses the Function of Hematopoietic Transcription Factors in Acute Myeloid Leukemia. Molecular Cell. 2015; 58:1028–36. [PubMed: 25982114]
66. Huang B, Yang XD, Zhou MM, Ozato K, Chen LF. Brd4 coactivates transcriptional activation of NF- kappaB via specific binding to acetylated RelA. Mol Cell Biol. 2009; 29:1375–87. [PubMed: 19103749]
67. Ding N, Hah N, Yu RT, Sherman MH, Benner C, Leblanc M, et al. BRD4 is a novel therapeutic target for liver fibrosis. Proc Natl Acad Sci USA. 2015; 112:15713–8. [PubMed: 26644586]

68. Delmore JE, Issa GC, Lemieux ME, Rahl PB, Shi J, Jacobs HM, et al. BET bromodomain inhibition as a therapeutic strategy to target c-Myc. Cell. 2011; 146:904–17. [PubMed: 21889194]

69. Alsarraj J, Walker RC, Webster JD, Geiger TR, Crawford NP, Simpson RM, et al. Deletion of the proline-rich region of the murine metastasis susceptibility gene Brd4 promotes epithelial-to-mesenchymal transition- and stem cell-like conversion. Cancer Res. 2011; 71:3121–31. [PubMed: 21389092]

70. Fernandez P, Scaffidi P, Markert E, Lee JH, Rane S, Misteli T. Transformation resistance in a premature aging disorder identifies a tumor-protective function of BRD4. Cell Rep. 2014; 9:248–60. [PubMed: 25284786]

71. Bolden JE, Tasdemir N, Dow LE, van Es JH, Wilkinson JE, Zhao Z, et al. Inducible In Vivo Silencing of Brd4 Identifies Potential Toxicities of Sustained BET Protein Inhibition. Cell Rep. 2014; 8:1919–29. [PubMed: 25242322]

72. Wu SY, Lee AY, Lai HT, Zhang H, Chiang CM. Phospho switch triggers Brd4 chromatin binding and activator recruitment for gene-specific targeting. Mol Cell. 2013; 49:843–57. [PubMed: 23317504]

73. Hinkal GW, Gatza CE, Parikh N, Donehower LA. Altered senescence, apoptosis, and DNA damage response in a mutant p53 model of accelerated aging. Mech Dev Ageing. 2009; 130:262–71.

74. Menck K, Behme D, Pantke M, Reiling N, Binder C, Pukrop T, Klemm F. Isolation of human monocytes by double gradient centrifugation and their differentiation to macrophages in teflon-coated cell culture bags. J Vis Exp. 2014; 91:e51554. [PubMed: 25226391]

75. Jaguin M, Houlbert N, Fardel O, Lecureur V. Polarization profiles of human M-CSF-generated macrophages and comparison of M1-markers in classically activated macrophages from GM-CSF and M-CSF origin. Cell Immunol. 2013; 281:51–61. [PubMed: 23454681]

76. Joshi AD, Oak SR, Hartigan AJ, Finn WG, Kunkel SL, Duffy KE, et al. Interleukin-33 contributes to both M1 and M2 chemokine marker expression in human macrophages. BMC Immunol. 2010; 11:52. [PubMed: 20958987]

77. McLean CY, Bristor D, Hiller M, Clarke SL, Schaar BT, Lowe CB, et al. GREAT improves functional interpretation of cis-regulatory regions. Nat Biotechnol. 2010; 28:495–501. [PubMed: 20436461]

Significance

This study reveals how cells undergoing oncogene-induced senescence acquire a distinctive enhancer landscape that includes formation of super-enhancers adjacent to immune modulatory genes required for paracrine immune activation. This process links BRD4 and super-enhancers to a tumor suppressive immune surveillance program that can be disrupted by small molecule BET inhibitors.

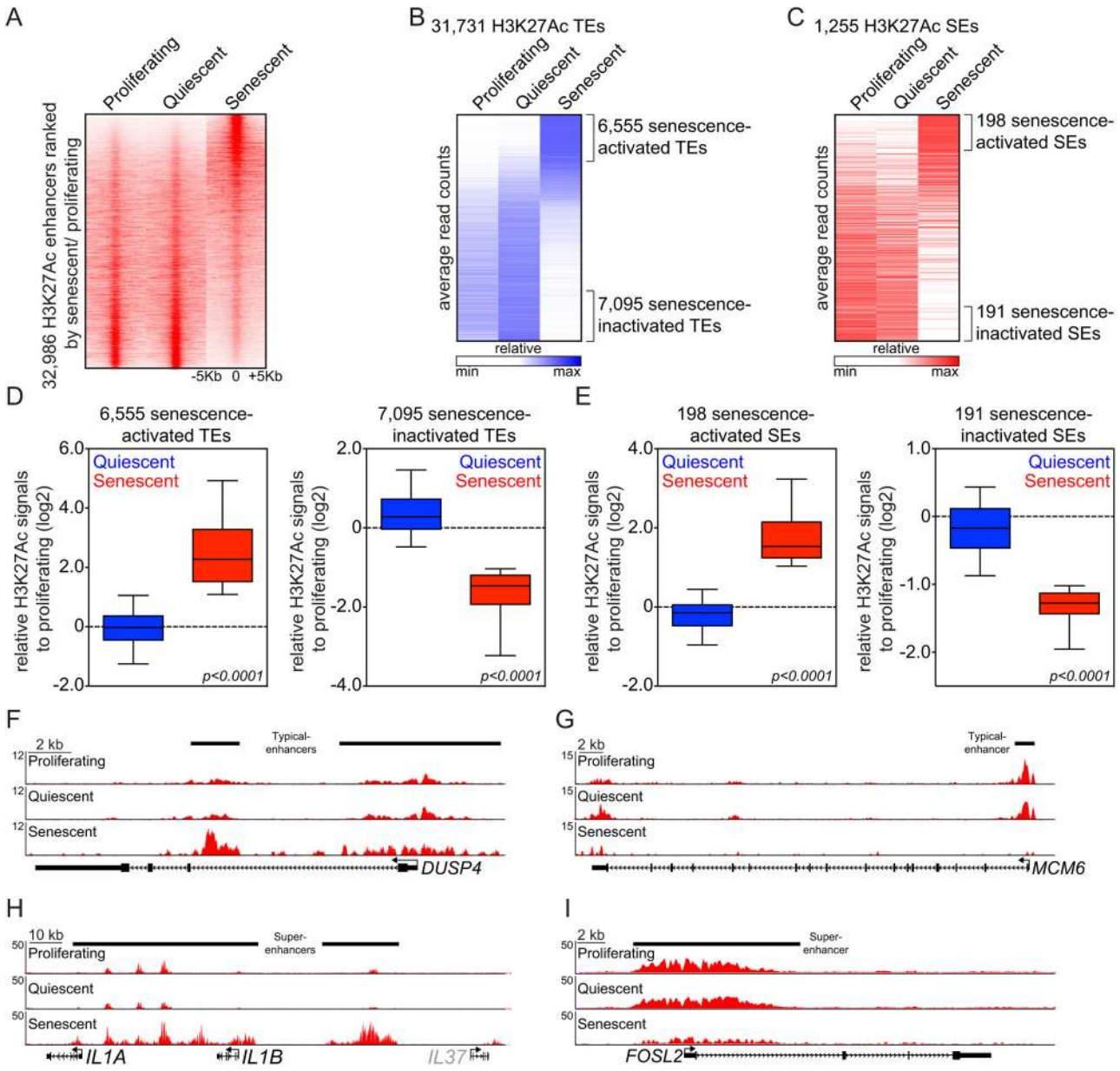

Figure 1. OIS is accompanied by global remodeling of enhancers

(A) Heat maps showing H3K27Ac ChIP-Seq signals over the 32,986 H3K27Ac-enriched union enhancers identified in proliferating, quiescent and senescent IMR90 cells. Rows correspond to ±5Kb regions across the midpoint of each H3K27Ac-enriched union enhancer, ranked by increased H3K27Ac signal in senescent cells versus proliferating cells. Color shading corresponds to the H3K27Ac ChIP-Seq read count in each region.

(B and C) Heat maps illustrating average read counts (normalized for total number of reads per region) of H3K27Ac signals over ± 5-Kb regions centered around 31,731 typical enhancers (TEs) (B) and 1,255 super-enhancers (SEs) (C) in the indicated conditions. Senescence-activated or -inactivated enhancers marked by brackets were defined as

H3K27Ac-enriched union enhancer regions exhibiting a greater or less than two fold change in H3K27Ac signals in senescence versus proliferating cells, respectively.
(D and E) Box plots showing relative changes in H3K27Ac signals in the indicated enhancer regions from quiescent (blue) and senescent (red) cells when compared to proliferating counterparts. Senescence-activated or -inactivated TEs (D) and SEs (E) were defined as described above. Fold changes with log2 scale (y-axis) were calculated by dividing H3K27Ac tag counts from quiescent or senescent conditions by H3K27Ac tag counts from proliferating condition. Significance was determined using a two-tailed t test. (F–I) H3K27Ac ChIP-Seq occupancy profiles at representative loci of senescence-activated (F and H) and senescence-inactivated (G and I) TEs (F and G) or SEs (H and I). Black bars above gene tracks denote TEs or SEs. Grey color on *IL37* gene indicates it is not substantially expressed based on RNA-Seq data.

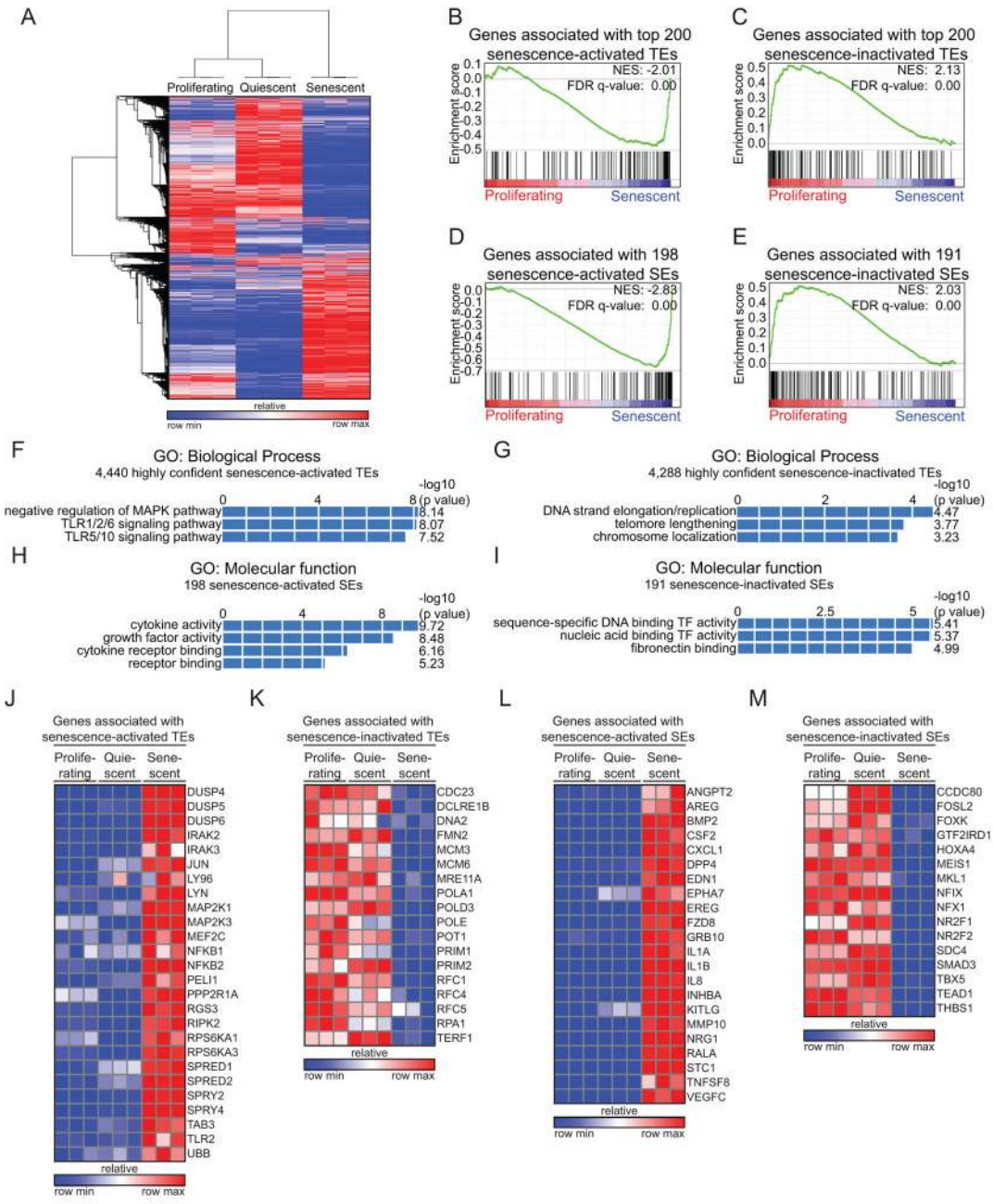

Figure 2. Enhancer remodeling during OIS is associated with a unique gene expression program

(A) Heat map of unsupervised hierarchical clustering from RNA-Seq data.

(B–E) Gene Set Enrichment Analyses (GSEA) comparing the expression of genes associated with senescence-activated or senescent inactivated typical enhancers (TEs) or super enhancers (SEs) between proliferating and senescent cells. Genes with the closest transcriptional start site (TSS) from H3K27Ac binding sites were considered as enhancer-associated genes. Each signature was defined from top 200 senescence-activated (B) and -inactivated (C) TEs, or 198 senescence-activated (D) and 191 inactivated (E) SEs. Genes were rank ordered according to their fold change between proliferating and senescent

conditions, as determined by their averaged RNA-Seq reads across three biological replicates per condition. NES, normalized enrichment score; FDR, false-discovery rate.
(F–I) GREAT gene ontology (GO) analyses of the genes associated with highly confident H3K27Ac binding sites for each of the indicated class of enhancers, activated (F and H) or inactivated (G and I) during senescence. Enhancers with tag counts >40 in senescent (F and H) or proliferating conditions (G and I) were considered as highly confident regions for H3K27Ac binding.
(J–M) Heat maps showing normalized expression of genes associated with the indicated senescence-activated or senescent inactivated TEs and SEs in proliferating, quiescent and senescent cells. The list of genes for each panel was extracted from GO analyses of Fig. 2F–2I.

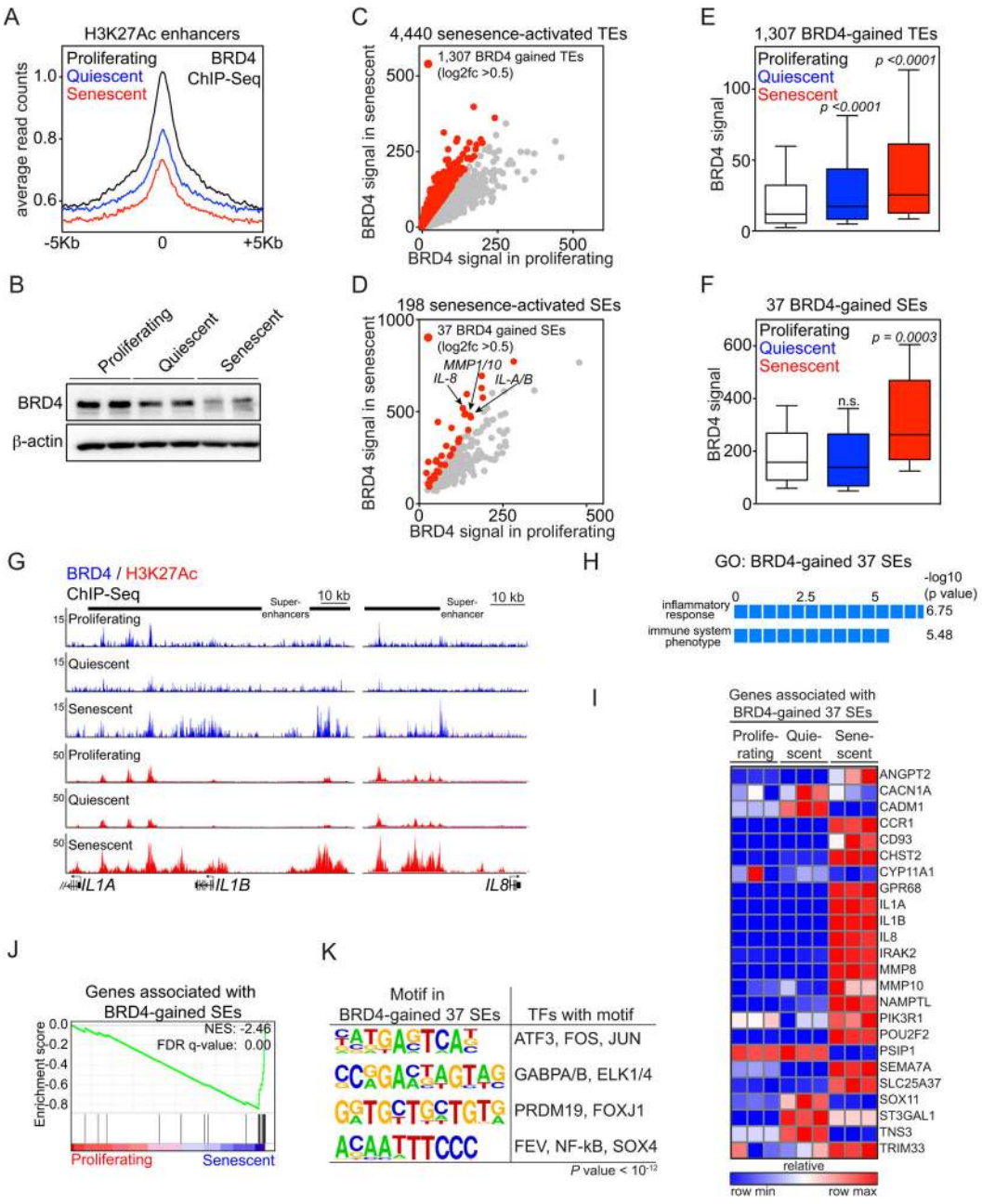

Figure 3. BRD4 is recruited to senescence-activated SEs associated with SASP genes

(A) BRD4 ChIP-Seq enrichment meta-profiles in proliferating (black), quiescent (blue) and senescent (red) IMR90 cells, representing the average read counts per 20-bp bin across a 5-Kb window centered on all 32,986 union H3K27Ac enhancers.

(B) Immunoblot analysis of BRD4 and β-actin (loading control) in whole cell lysates from proliferating, quiescent and senescent cells.

(C and D) Scatterplots of absolute BRD4 signals (tag counts) at senescence-activated TEs (C) or SEs (D) in proliferating (x-axis) and senescent (y-axis) cells. The 1,307 TEs and 37 SEs showing a greater than 0.5 fold change (log2 scale) in BRD4 signals in senescence

versus proliferating cells are marked in red. (E and F) Box plots of absolute BRD4 signals at the indicated enhancer loci in proliferating (white), quiescent (blue) or senescent (red) cells. P-values were calculated by comparing absolute BRD4 ChIP-Seq signals at 1,307 BRD4-gained TEs (E) or 37 BRD4-gained SEs (F) in proliferating cells versus quiescent or senescent counterparts using a two-tailed t-test. Normalized tag counts of the BRD4 ChIP-Seq is provided in Table S2.

(G) ChIP-Seq occupancy profiles for BRD4 (blue) and H3K27Ac (red) at *IL1A*/*IL1B* and *IL8* locus at indicated conditions. Black bars above gene tracks denote SEs. The *IL1A* and *IL1B* H3K27Ac plots are data from Fig. 1H.

(H) GREAT GO analysis of 37 BRD4-gained SEs.

(I) Heat map showing the relative expression of genes associated with the 37 BRD4-gained senescence-activated SEs in proliferating, quiescent or senescent IMR90 cells.

(J) GSEA of the genes associated with 37 BRD4-gained SEs with proliferating and senescent conditions. Genes associated with BRD4 binding sites were defined as described in Fig. 2.

(K) Motif analysis of 37 BRD4-gained SEs for putative transcription factor binding sites. A 1-Kb region centered on BRD4 peaks was used for motif discovery. Motifs with p-value less than 10^{-12} were considered as significant candidates.

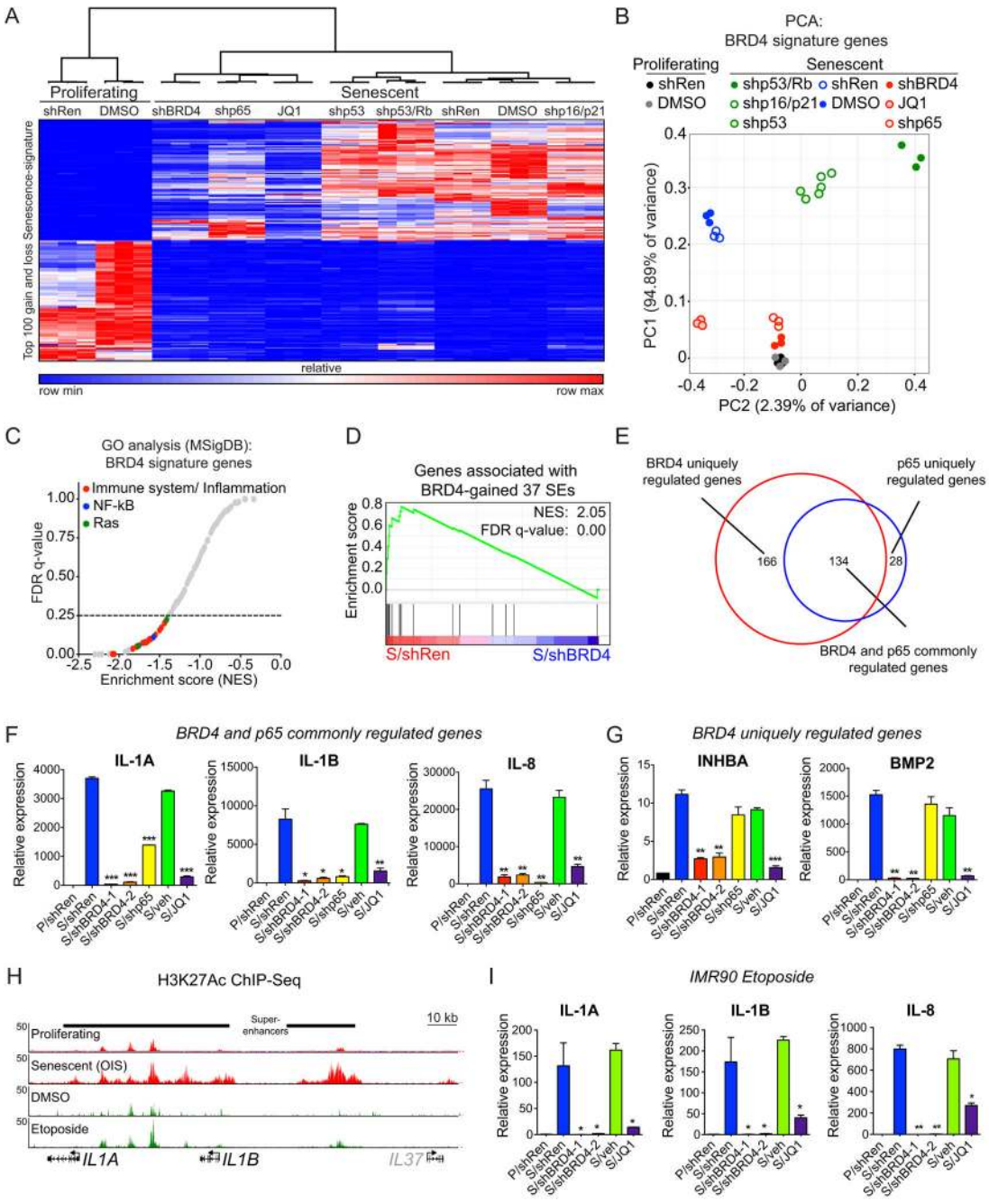

Figure 4. BRD4 bromodomain is critical for expression of SASP genes

(A) Heat map of supervised hierarchical clustering from RNA-Seq data. Senescence gain- and loss- signatures correspond to top 100 genes that display more than two fold change in senescent (but not in quiescent) cells as compared to proliferating condition. Expression values (rpkm) of combined 200 senescent-signature genes in the indicated conditions were subjected to clustering based on one minus Pearson correlation test.

(B) Supervised principal component analysis (PCA) of BRD4 gene expression signature for the indicated conditions. BRD4 signature was defined by identifying senescent-activated genes that displayed more than two fold decrease with shBRD4 expression.
(C) GSEA on the RNA-Seq data of BRD4 signature genes. 210 gene sets available from the Molecular Signature Database (size of gene set; min=15, max=500) were used in the analysis. From 210 gene sets tested, only 24 gene sets were considered as statistically significant (FDR<25%). Similar gene sets were collapsed as representative groups, including immune system/inflammation-related pathways (red), NF-κB signaling pathway (blue) and Ras-signaling pathway (green).
(D) GSEA of 37 BRD4-gained SE signature following shRen or shBRD4 expression.
(E) Area-proportional Venn diagram showing overlap between senescence-activated genes regulated by BRD4 (red) or p65 (blue).
(F, G) qRT-PCR analyses of the indicated SASP factors in proliferating (P) or senescent (S) cells expressing shRNAs targeting Renilla (neutral control), BRD4 or p65, or treated with vehicle (veh) or JQ1. Shown are representative senescence-activated SASP genes exhibiting BRD4 and p65 co-dependency (F), or only BRD4-dependency (G). See Supplementary Figs. S3C and S3D for additional examples. Data are represented as mean ± standard deviation (SD) of two biological replicates.
(H) H3K27Ac ChIP-Seq occupancy profiles showing gain of H3K27Ac-marked SEs associated with the indicated SASP genes in two senescence conditions triggered by different stimuli. The OIS H3K27Ac mark plots are data from Fig. 1H.
(I) qRT-PCR analyses of the indicated SASP factors in proliferating (P) or senescent (S) cells expressing shRNAs targeting Renilla (neutral control) or BRD4, or treated with vehicle (veh) or JQ1. Senescence was induced by etoposide treatment. See Supplementary Fig. S5C for additional senescence-activated SASP genes exhibiting BRD4-dependency in the context of etoposide-induced senescence. Data are represented as mean ± standard deviation (SD) of two biological replicates.

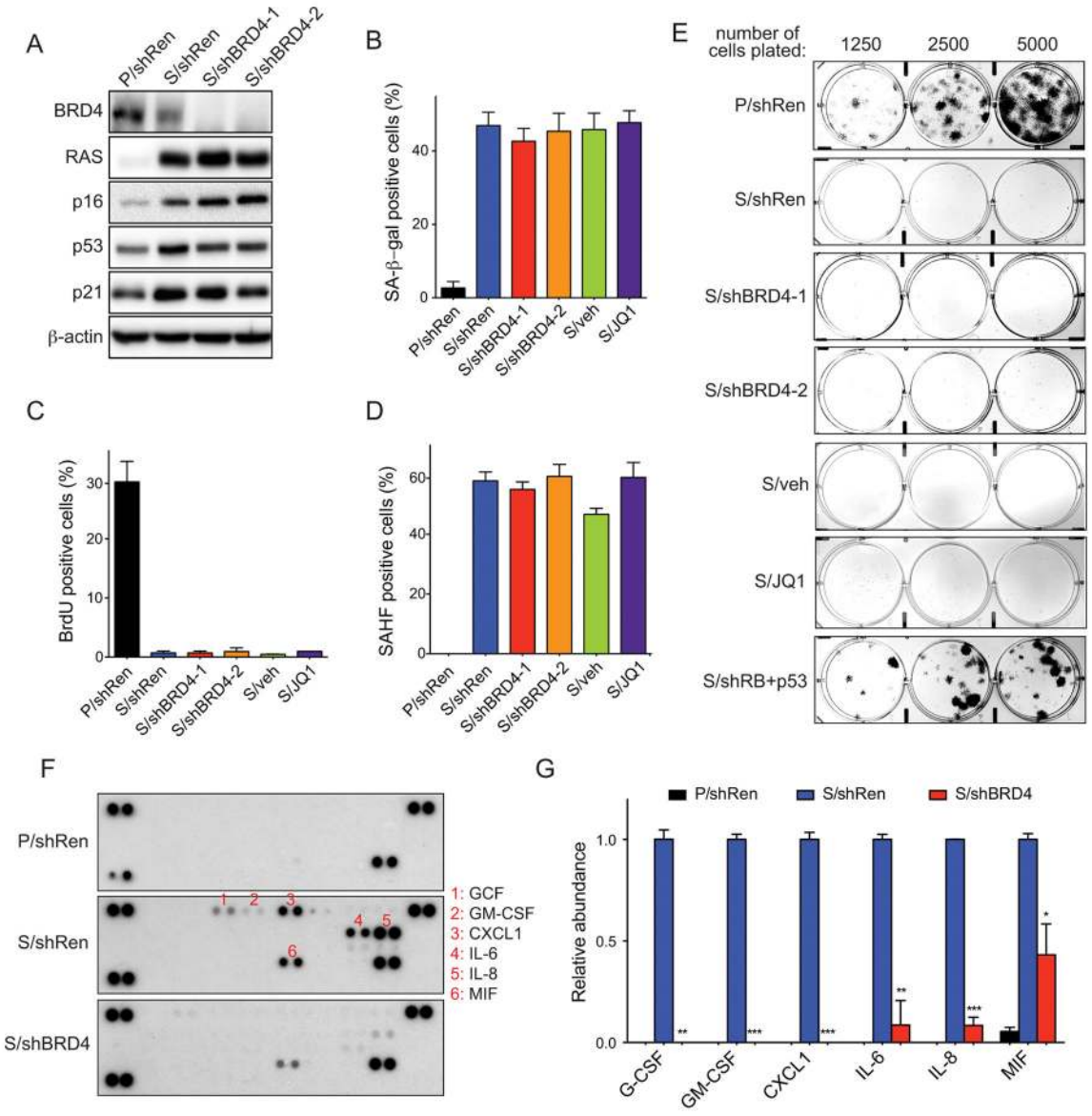

Figure 5. BRD4 is indispensable for the production of senescence-associated secretome but not for the cell cycle arrest

(A) Immunoblot analyses of the indicated proteins in whole cell lysates of proliferating (P) or senescent (S) IMR90 cells expressing shRNAs against BRD4 (shBRD4) or Renilla (shRen, neutral control). Senescence was induced by H-Ras^{G12D} expression. β-actin was used as loading control.

(B) Quantification of SA-β-gal staining in proliferating (P) or senescent (S) IMR90 cells expressing the indicated shRNAs, or treated with JQ1 or vehicle (veh). Data are presented as means ± SD of two independent experiments.

(C and D) Quantification of BrdU incorporation (C) and SAHF formation (D) in proliferating (P) or senescent (S) IMR90 cells expressing the indicated shRNAs, or treated with JQ1 or vehicle (veh). Data are presented as means ± SD of two independent experiments.

(E) Colony formation assays documenting the impact of inactivating BRD4 on the ability of H-Ras^{V12}-expressing IMR90 cells to grow at low density. Shown are representative crystal violet stainings of 6-cm plates 2 weeks after plating. Proliferating (P) and senescent (S) cells expressing a tandem Rb and p53 shRNA (S/shRb+p53; expected to bypass senescence) were used as control.

(F and G) Cytokine array analysis of conditioned media analysis from proliferating (P) or senescent (S) IMR90 cells expressing the indicated shRNAs (F) and relative quantification (G). Data are presented as means ± SD of two independent experiments.

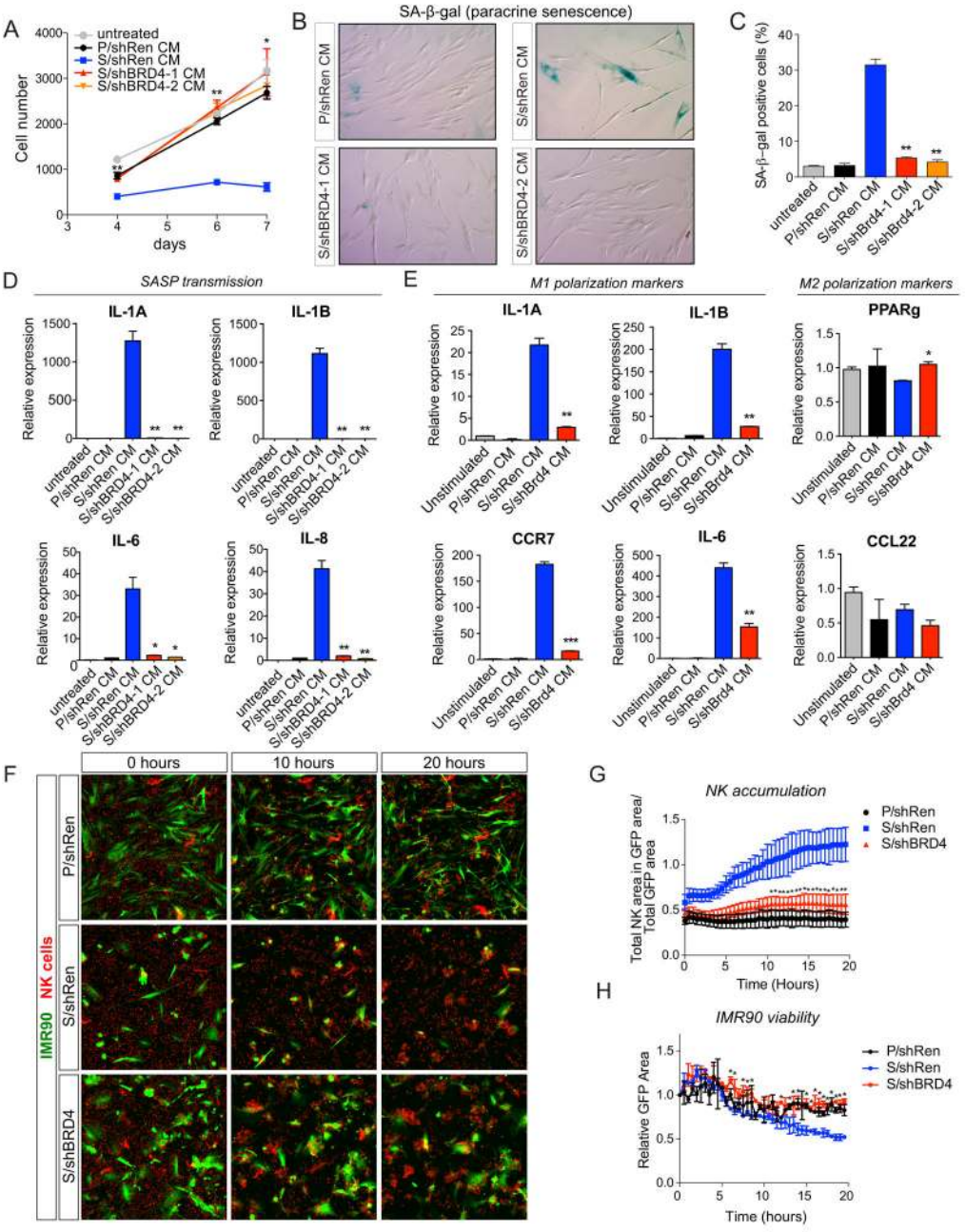

Figure 6. BRD4 mediates paracrine senescence and SASP-triggered immune cell activation *in vitro*

(A) Proliferation of naïve IMR90 cells, untreated or subjected to conditioned media (CM) from proliferating (P) or senescent (S) IMR90 cells expressing the indicated shRNAs, as a measure of SASP-induced paracrine senescence.

(B) Representative micrographs of the same cell populations as in (A) stained for SA-β-gal activity after a 7-day exposure to the indicated CM.

(C) Quantification of the percentage of naïve IMR90 cells staining positive for SA-β-gal activity following a 7-day exposure to CM from proliferating (P) or senescent (S) cells

expressing the indicated shRNAs. Data correspond to the mean ± SD of two independent experiments.

(D) qRT-PCR analysis of SASP gene expression in naïve IMR90 cells exposed to the indicated CM. Data correspond to the mean ± SD of two independent experiments.

(E) qRT-PCR analysis of M1 (left panels) or M2 (right panels) polarization markers in human monocyte-derived macrophages exposed to CM from proliferating (P) or senescent (S) cells expressing the indicated shRNAs.

(F) Representative micrographs of co-cultures of NK cells (red) with proliferating (P) or senescent (S) IMR90 cells expressing the indicated GFP-linked shRNAs. Note the rapid NK cell-mediated elimination of senescent cells expressing the neutral shRNA against Ren (shRen).

(G) Quantification of NK cell “targeting” of IMR90 cells. NK cell attraction to the indicated IMR90 cell populations was quantified at the indicated time points by automated detection of the total IMR90 cell area covered by NK cells.

(H) Quantification of IMR90 viability over time in NK-IMR90 co-cultures. The viability of IMR90 cells expressing the indicated GFP-linked shRNAs was quantified at the indicated time points by automated high-throughput detection of GFP positive signals (see Supplemental Experimental Procedures for additional details), and expressed normalized to GFP values at time point zero. Data correspond to means ± SEM of 2 biological replicates, 4 adjacent fields per well were analyzed per replicate, per condition.

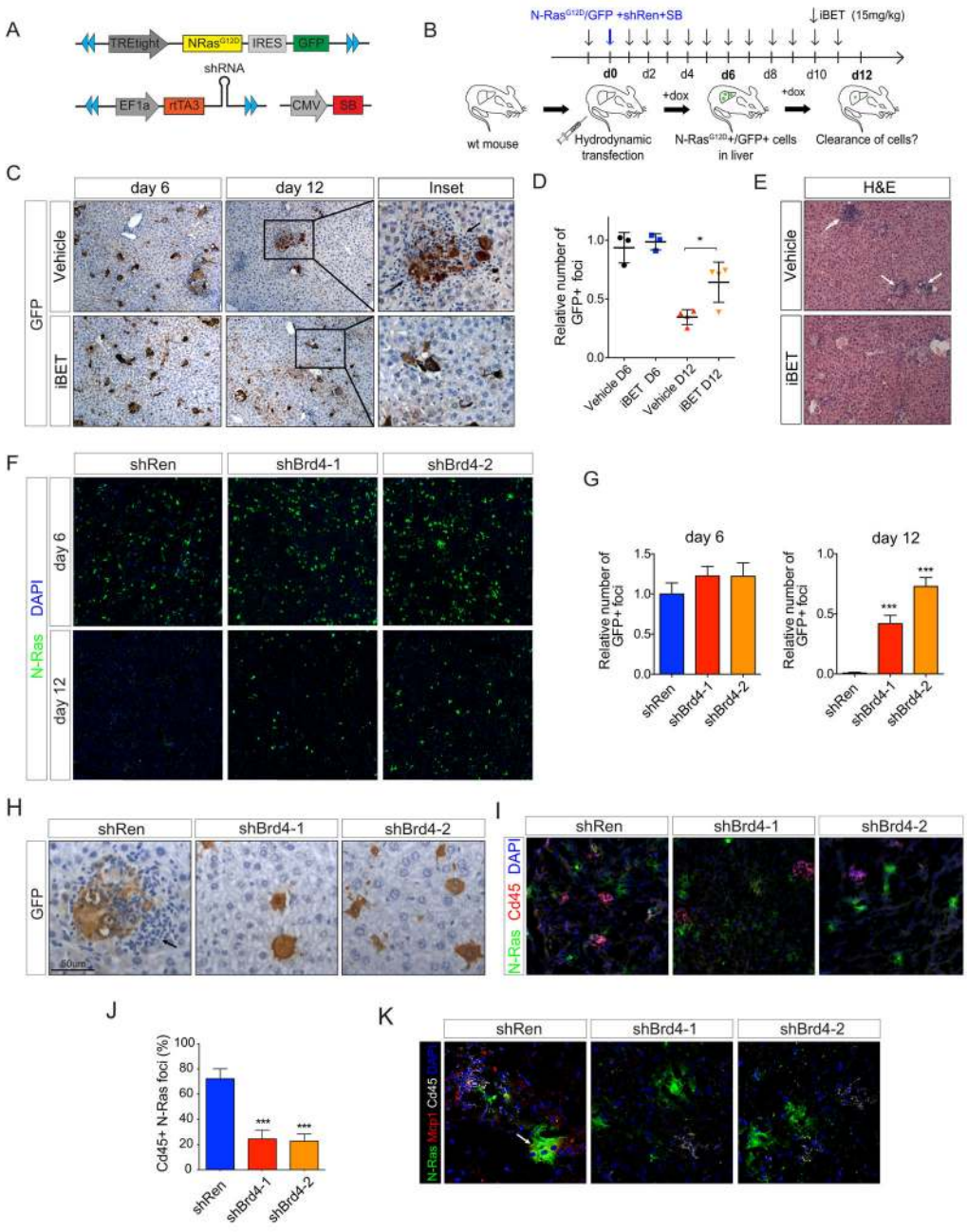

Figure 7. Brd4 inhibition impairs immune surveillance of oncogenic N-Ras expressing senescent cells *in vivo*

(A) A schematic diagram of the three sleeping beauty constructs used in the hydrodynamic transfection experiments. The blue triangles indicate the sleeping beauty direct and inverted repeats. SB: Sleeping Beauty transposase.

(B) Experimental strategy to address the impact of systemic Brd4 inhibition on clearance of senescent hepatocytes. Mice were injected with the indicated constructs through hydrodynamic transfection and treated with I-BET 762 (iBET) or vehicle orally every day (15mg/kg). Livers were harvested at days 6 and 12 and subjected to histological analyses to assess the extent of immune-mediated senescent hepatocyte clearance (see Figs. C–E). The

same vector system and timeline was used for hepatocyte-specific Brd4 depletion using shRNAs against Brd4 (see Figs. F–L). Figure adapted from ref. [35].

(C) Representative immunohistochemistry (IHC) stainings for GFP on liver sections harvested from vehicle or iBET-treated mice at day 6 and 12 post-transduction of $NRas^{G12D}$-IRES-GFP by hydrodynamic injection. Arrows point to clusters of immune infiltrates.

(D) Quantification of the number of GFP positive foci in livers from vehicle or iBET-treated mice at the indicated time points post-injection. Each dot represents the mean numbers of GFP+ foci per mouse (ten 10X fields quantified/mouse) and results are expressed relative to vehicle-day 6 mean value. Means ± SD values for each experimental group are also indicated.

(E) Representative H&E staining of livers from vehicle or iBET-treated mice harvested at day 12 post-injection. Arrows point to clusters of immune infiltrates.

(F) Representative immunofluorescence (IF) for N-Ras (green) on day 6 (top panels) or day 12 (bottom panels) liver tissue sections from mice injected with transposon-based vectors encoding for oncogenic N-Ras- and indicated shRNAs. Nuclei are counterstained with DAPI.

(G) Bar graphs show corresponding quantifications of the number of N-Ras+ cells per field, at day 6 or day 12 post-injections. Data are presented as mean + S.D. (n=4) from thirty 10X fields per mouse. Results are presented as number of GFP positive foci relative to control shRNA on day 6.

(H) Immunohistochemistry (IHC) staining for GFP on day 6 liver tissues from mice injected with transposon-based vectors encoding for oncogenic N-Ras and indicated shRNAs. Hematoxylin was used for counterstaining. GFP marks hepatocytes co-expressing N-Ras and the indicated shRNAs. Arrows indicate immune infiltrates surrounding N-Ras/shRen-expressing GFP positive foci.

(I) Co-immunofluorescence for N-Ras (green) and CD45 (red) on frozen liver tissue sections harvested on day 6. Nuclei are counterstained with DAPI.

(J) Bar graphs show corresponding quantifications of the percentage of N-Ras foci infiltrated by CD45+ cells at day 6. Data are presented as mean + S.D. (n=4) from thirty 10X fields per mouse.

(K) Triple-immunofluorescence for N-Ras (green), Cd45 (white) and the SASP factor Mcp1 (red) on frozen liver tissue sections harvested on day 6. Nuclei are counterstained with DAPI. Arrows point to N-Ras/shRen-expressing foci exhibiting induced levels of the secreted chemokine Mcp1.